R. & M. No. 3193
(20,920)
A.R.C. Technical Report

R. & M. No. 3193

MINISTRY OF AVIATION

AERONAUTICAL RESEARCH COUNCIL
REPORTS AND MEMORANDA

A Free-Flight Investigation into the Effect of Body Shaping on the Zero-Lift Drag of a Wing–Body Combination at Transonic and Supersonic Speeds

By J. A. Hamilton, G. H. Greenwood, and W. T. Lord

LONDON: HER MAJESTY'S STATIONERY OFFICE
1961
PRICE 15*s.* 0*d.* NET

A Free-Flight Investigation into the Effect of Body Shaping on the Zero-Lift Drag of a Wing–Body Combination at Transonic and Supersonic Speeds

By J. A. Hamilton, G. H. Greenwood, and W. T. Lord

Communicated by The Deputy Controller Aircraft (Research and Development)
Ministry of Supply

*Reports and Memoranda No. 3193**
September, 1958

Summary. This report describes a series of free-flight tests designed to investigate various methods of body shaping to achieve low drag at transonic and supersonic speeds. In all, ten configurations were flown; three had unwaisted bodies, five were designed by area-rule methods and two were designed to achieve a specified pressure distribution in the wing–body junction. All the models had identical values of total volume (wing + body), body length and body base area; the wing design was also common (45 deg sweep, aspect ratio 2·4, thickness/chord ratio 0·074, no taper). The Mach number range covered was from 0·8 to 1·5.

The area-rule models gave results which followed closely the design trends indicated by area-rule theory. The models designed to achieve specified pressure distributions gave a sonic-drag reduction of about 20 per cent compared with the unwaisted models, a smaller improvement than would have been expected if their full potential benefit had been achieved.

1. *Introduction.* When the investigation described in this report was initiated a number of theoretical studies had been made at the Royal Aircraft Establishment to demonstrate the design implications of the sonic and supersonic area rules. The initial aim of the experimental programme was to provide a definitive background of measured drag information against which these theoretical implications could be assessed.

In designing models for this programme, current design trends were borne in mind but the need to achieve a relatively simple and yet unequivocal experiment was regarded as paramount. Thus, the wing geometry was chosen in such a manner that the application of area-rule design methods would give drag differences which were large enough to be measured unambiguously using standard free-flight techniques. The body geometry was largely dictated by the space needed to accommodate propulsion motors and telemetry equipment. The resulting configurations depart appreciably from the slenderness assumptions implicit in linearised supersonic-flow theory, and the critical Mach number 1·08 of the equivalent sheared wing is rather close to unity. Nevertheless, the available

* R.A.E. Report Aero. 2611, received 8th April, 1959.

empirical evidence in this report and others (*e.g.*, Ref. 1) suggests that area-rule theory is capable of yielding plausible design trends even with such configurations.

In addition to the area-rule series, one or two models were designed using the body-shaping principles due largely to Küchemann and Hartley[2]. Thus all the designs are based on linearised supersonic theory, but the theory is applied in different ways.

2. *General Description of the Investigation.* 2.1. *Model Design.*—The tests were confined to one basic configuration, consisting of an untapered wing mounted on a central fuselage (Fig. 1). Only the shape of the fuselage was modified in various ways, the wing remaining the same. For the area-rule designs this restriction is, theoretically, of no consequence, but for those body shapes which were designed to have a specific junction pressure distribution, only the wing-root pressures are considered and one could argue that tip effects, for example, may frustrate the purpose of the junction design. The restriction to fuselage modifications is justified for such applications by the argument (Ref. 2) that in the transonic and low-supersonic speed ranges, the normal-pressure drag at zero lift is confined to the region of the wing root so that fuselage shaping alone can be used to produce a pressure field which can interfere favourably with that of the wing and thus reduce the drag in the region which matters most.

To provide an unequivocal basis for drag comparison between models, all the designs had:

(i) The same gross wing geometry:

Sweepback	= 45 deg
Aspect ratio	= 2·40
Thickness/chord ratio	= 0·074
Section shape	= parabolic biconvex
Taper ratio	= 1·00

(ii) the same total volume (wing + body)

(iii) the same body length

(iv) the same body base area,

the last three being determined by the volume, length, and base area required to accommodate the rocket motor in the non-separating models.

Within these basic limitations ten different body shapes were tested: summarised descriptions of these are given in Table 1, body ordinates in Table 2 and the design methods are detailed in Appendix I. The various body shapes, area distributions, models, etc., are illustrated in Figs. 4 to 6.

Briefly, the models fall into three groups:

(*a*) Models 1 to 4 to investigate sonic area rule (Figs. 4a, 5a and 6a).

(*b*) Models 8 to 10 to investigate the achievement of low drag by designing for a specified pressure distribution in the wing–body junction[2] (Figs. 4b, 5b and 6b).

(*c*) Models 5s to 7s to investigate supersonic area rule (Figs. 4c, 5c and 6c).

In addition to this main programme a measurement was made of the drag of the common wing 'in isolation' by mounting it upon a standard parallel-sided body of known drag and measuring the drag of the combination (Fig. 7).

All the models were fitted with small fins to provide directional stability; these were not included in the theoretical design calculations but allowance has been made for their drag in the comparisons between experiment and theory.

2.2. *Test Technique.* In terms of free-flight technique the models fall into two categories:

(*a*) *Non-separating models.*—In these, the rocket motor forms an integral part of the structure (Figs. 1 and 2), giving a test vehicle which is simple to design and operate. However, to accommodate the body waisting necessary for these tests the motor had to be clothed in a wooden fairing and the model weight limited the maximum Mach number to about 1·2.

(*b*) *Separating models.*—These models had an external rocket motor which fell away as soon as maximum velocity had been achieved. They were able to cover a Mach number range from 0·9 to 1·5 and were used primarily for the supersonic-area-rule investigation (Figs. 1 and 3). The separating models were half the size of the non-separating models.

A general description of the ground and airborne instrumentation employed in free-flight trials at the R.A.E. is given in Ref. 3. For these particular tests:

Trajectory was obtained from kine-theodolite measurements.

Velocity was measured by a radio-Doppler system.

Drag was obtained by differentiation of the Doppler record and also from an accelerometer measurement in the model.

Base pressure was measured by pressure transducers in the model (Appendix III).

3. *Assessment of the Reliability of the Experimental Results.* The accepted figures for the accuracy of free-flight determination of zero-lift drag are ± 5 per cent at supersonic speeds and ± 10 to 15 per cent at subsonic speeds, the higher figure being a reflection of the small proportion of the instrument range utilised at low speed. The subsonic figure may be improved if a good Doppler measurement is available in this region. In general, the agreement between drag derived from Doppler measurements and drag derived from accelerometer measurements was within these limits (Fig. 8 is typical).

At various points in the programme a check on the overall reliability was made by firing repeat models of the same design, and two designs were flown both in separating and non-separating versions. Comparative plots are given in Figs. 9 to 13, and these confirm the accepted accuracy limits. Particularly noteworthy is the comparison between separating and non-separating models (Figs. 11 and 12) wherein the experiment has apparently confirmed the difference in skin-friction drag between the two sets of models. However, this is of the same order as the experimental accuracy and the result may be fortuitous.

One final guide to reliability is provided by comparing subsonic drags. For the non-separating models an appreciable range of subsonic Mach number is available and the scatter is within the accepted value of ± 10 per cent (Figs. 14 and 15). Because of their greater maximum speed and hence greater distance to reach subsonic speed, less subsonic drag range is available from the separating models (some failed to reach the subsonic drag level) but the agreement is apparently equally good (Fig. 17).

4. *Discussion.* For ease of discussion the experimental results have been divided into three groups:

In Fig. 14: The effect of sonic area rule

In Fig. 15: Comparison between the area-rule and other design criteria

In Fig. 17: The effect of area-rule design Mach number.

The very large reductions in sonic drag produced by application of the sonic area rule are now an accepted feature of transonic aerodynamic design: the results illustrated in Fig. 14 amply confirm these effects and also show a close equality in sonic drag rise between the wing–body combination (Model 3) and its equivalent body (Model 4).

Less familiar are the comparisons between the sonic-area-rule, 'sheared-wing' and 'zero-C_p' designs presented in Fig. 15. Before considering these in detail, an interpolated comment on the bases of the 'sheared-wing' and 'zero-C_p' designs may be appropriate. The concept put forward by Küchemann and Hartley, *e.g.*, in Ref. 2, is that the only satisfactory method of designing wing–body combinations involves the calculation not only of the overall drag but also of wing and body shapes to give a specified pressure distribution everywhere which can be achieved in a real flow. There being as yet no general method to perform such a calculation, they go on to show that at transonic and low supersonic speeds the normal-pressure drag at zero lift is mainly confined to the wing root and hence that modifications to the wing–body junction only, could bring about reductions in drag. Among the desirable junction pressure distributions considered in Ref. 2 are constant pressure equal to the free-stream pressure ('zero-C_p' design) and the pressure distribution of the infinite sheared wing ('sheared-wing' design), the latter ensuring at the same time that the flow can be sub-critical and that the pressure drag of the wing is zero. At the time of designing the present models, numerical methods were available only to calculate the pressure distribution at the centre section of a swept wing and along the junction between wing and body by means of linearised theory; the calculation of pressures on the wing away from the junction and over the body presented difficulties (Appendix I).

Returning now to Fig. 15, the most striking result is the equality in drag of the two sonic-area-rule models, one (Model 3) having circular-body cross-sections, the other (Model 10) having eliptical-body cross-sections with no waisting at all in the plane of the wing. Since these two had the same sonic area distribution one would have expected equality of drag at sonic speed; in the event, the drags are equal over the whole Mach-number range tested. If, however, one assumes as did the early numerical methods for estimating junction pressure, that only the shape of the body in the wing plane is important, one would have expected a much higher drag result from Model 10, approaching that of Models 1 and 2 (Fig. 14).

This result serves to confirm that, in contrast to experience at subsonic speeds, the shape of the cross-section of the body must affect the pressure distribution on the wing and that calculations involving the wing plane only may be misleading. In the light of this fact, Bagley has subsequently shown in some unpublished work that a quasi-cylinder theory based on non-circular cross-sections predicts changes in junction pressure distribution of the right order and trend even when, as in Model 10, the body shaping is applied away from the junction.

Junction-pressure calculations for Models 3 and 10 are given in Fig. 24b and there compared with the 'sheared-wing' and 'wing-alone' pressure distributions. For Model 10 the early numerical method (no allowance for body cross-section shape) would have suggested a pressure distribution akin to that of the 'wing-alone' curve in Fig. 24b. When shape effects are included, the predicted pressure distribution becomes similar in character to that of the infinite sheared wing. Thus the experimental fact of the drag equality of Models 3 and 10 is less at variance with the pressure-distribution criteria for low drag than the original pressure estimates would have suggested.

The performance of the 'zero-C_p' and 'sheared-wing' designs is qualitatively in accord with area-rule theory (Fig. 15). Their sonic area distributions are less smooth than those of the sonic-area-rule designs (Fig. 5b), the 'sheared-wing' being the better of the two. Carrying this qualitative argument a little further, Fig. 16 shows that the drag of the 'sheared-wing' design is almost the same as that of the area-rule design for $M = 1{\cdot}08$ (the 'sheared-wing' design Mach number was $M = 1{\cdot}05$) and Fig. 5d shows a corresponding similarity between the sonic area distributions.

One point to be borne in mind when considering these two results is that, as discussed above, the 'sheared-wing' and 'zero-C_p' body junctions were calculated by means of a method which took no account of the shape of the body cross-section. Later calculations using the improved method due to Bagley indicate the possible magnitudes of the deviations from the specified pressure distributions (Fig. 24d). In the absence of any measurements to indicate how closely in fact the specified pressure distributions were achieved it is doubtful whether one can profitably discuss the merits and demerits of these designs in terms of what constitutes a suitable junction pressure distribution (*see also* Appendix IV).

For those models which were designed according to supersonic area rule, the general pattern of the supersonic drag variations follows that suggested by the theory (Figs. 17 and 21). The $M = 1{\cdot}41$ design has a lower drag than the 'conventional' design (Model 2) up to $M = 1{\cdot}6$, the maximum Mach number achieved, but the difference between the two is small and is of the same order as that suggested by area-rule theory for the interference drag of Model 2 (C_D (interference) $\approx 0{\cdot}002$). A more detailed examination of the relationship between estimate and measurement is made in the next Section.

To round off the general discussion of the results we consider briefly the effect of body shaping on drag-divergence Mach number. In this context the Mach number for drag divergence (M_D) has been defined as that at which the value of the slope $\partial C_D/\partial M$ reaches 0·01. For the transonic designs this criterion gives the following value of M_D:

Model	M_D
Sonic area-rule (3 and 10)	0·97
Sheared wing (9)	$0{\cdot}95_5$
$C_p = 0$ (8)	$0{\cdot}96_5$
Parallel body (1)	$0{\cdot}92_5$
Best body (2)	0·92
Equivalent body (4)	0·97

Thus there is little to choose in this connection between 'zero-C_p', 'sheared-wing' and sonic area-rule designs: all three give an improvement of 0·04 to 0·05 in M_D compared with the unwaisted bodies.

Increasing the design Mach number for area-rule application has an adverse effect on M_D, thus:

Area-rule design M	M_D
1·00	0·97
1·08	$0{\cdot}95_5$
1·17	0·94
1·41	0·92

i.e., the $M = 1{\cdot}41$ design is no better than the unwaisted designs.

5. *Comparison with Theoretical Predictions.* Theoretical values of wave drag for models 2, 3, 5s, 6s, 7s, 8 and 9 have been calculated at $M = 1{\cdot}0$, 1·08, 1·17 and 1·41 by the numerical method outlined in Appendix II. For the purpose of comparison between theory and experiment we have chosen to consider total zero-lift drags rather than wave drags; this is prompted principally by the

difficulties encountered in measuring base drag described in Appendix III. To do this involves an estimation of base drag, skin-friction drag, and fin drag. Base drag has been taken from Fig. 18, the derivation of which is described in Appendix III: skin-friction drag was estimated using the turbulent-boundary-layer values given in Ref. 4*: the fin drag was derived from measurements made on fins of similar geometry.

In considering these comparisons one must always have in mind the limitations of the flow assumptions and of the mathematical framework upon which area-rule theory is based. A rigorous interpretation would suggest that application to the model designs of the present tests must result in only fortuitous agreement between theory and experiment. However, there is by now an adequate body of experiment–theory comparison (Ref. 1, for example) to suggest that this is an unduly restrictive view, provided one excepts those regions where linearised theory has proved to be misleading even for more slender shapes, *e.g.*, at sonic speed and when the Mach angle approaches the wing sweepback angle. Equally, one should not try to read too much significance into the individual comparisons of Fig. 20: the primary purpose of the present investigations was to show that the design trends suggested by area-rule theory were correct. This is a less exacting requirement than the achievement of quantitative agreement between experiment and theory to within specified limits. The summary curves of Fig. 21 would suggest that this principal aim has been attained.

6. *Conclusions.*

(i) For those wing–body combinations designed according to sonic and supersonic area rules, the pattern of measured zero-lift drag variation with design Mach number and free-stream Mach number conformed closely to that suggested by area-rule theory.

(ii) The models designed according to sonic area rule revealed shortcomings, since rectified, in certain numerical methods for calculating wing–body junction pressure distributions.

(iii) A wing–body combination designed to have the infinite-sheared-wing pressure distribution in the junction at $M = 1{\cdot}05$ gave a higher drag than was expected at the design point. However, its zero-lift drag curve over the range $M = 1{\cdot}0$ to $1{\cdot}2$ was almost identical to that of an area-rule design for $M = 1{\cdot}08$.

(iv) A wing–body combination designed to have 'zero C_p' in the junction gave higher drags over the range $M = 1{\cdot}0$ to $1{\cdot}2$ than the 'sheared–wing' design.

(v) Altogether, it has been demonstrated that considerable reductions of the zero-lift wave drag in the transonic speed range can be achieved by favourable interference between the pressure field of a waisted body and a swept wing, even in a relatively difficult case where the configuration is not slender where the aspect ratio of the wing is relatively small and the basic critical Mach number is close to unity, so that the theoretical assumptions are not likely to be strictly satisfied.

---

* Because of the difference in size between the separating and non-separating models the estimated skin-friction drag-coefficient values differ by about 0·001 (*cf.*, Figs. 11 and 12). This amount is of the same order as the accuracy of the experimental drag determination and though there is some evidence of its presence in the experimental results we have used mean C_f values for the comparison between theory and experiment.

LIST OF SYMBOLS

C_{D0}	Drag coefficient at zero lift
C_{pb}	Base pressure coefficient $\frac{P_{base} - P_0}{q_0}$
L	Body length
M_0	Free-stream Mach number
M_D	Drag-divergence Mach number $\left(\frac{\partial C_D}{\partial M} = 0{\cdot}01\right)$
M_{Des}	Design Mach number (Area-rule)
$S(x)$	$\frac{\text{Cross-sectional area at } x}{L^2}$
x	$\frac{\text{Distance from body nose}}{L}$

LIST OF REFERENCES

No.	*Author*	*Title, etc.*
1	R. L. Nelson and C. J. Welsh ..	Some examples of the applications of the transonic and supersonic area-rules to the prediction of wave drag. N.A.C.A. Research Memo. L56011. TIL/5463. March, 1957.
2	D. Küchemann and D. E. Hartley	The design of swept wings and wing–body combinations at transonic speeds. A.R.C. 17,871. April, 1955.
3	J. A. Hamilton and P. A. Hufton	Free-flight techniques for high-speed aerodynamic research. *J. R. Ae. Soc.* March, 1956.
4	.. ..	*R. Ae. Soc.* Data Sheets.
5	R. T. Jones	Theory of wing–body drag at supersonic speeds. N.A.C.A. Research Memo. A53H18a. TIB/3890. A.R.C. 16,603. September, 1953.
6	E. Eminton	On the minimisation and numerical evaluation of wave drag. A.R.C. 19,212. November, 1955.
7	J. A. Bagley	Some aerodynamic principles for the design of swept wings. (To be published in *Progress in the Aeronautical Sciences*. Pergamon Press, London.)

APPENDIX I

Details of the Design Methods

The detailed thinking behind the designs investigated in this report has been described in three papers by Lord and Bagley. Since these are not generally available, the salient points have been summarised in this appendix*.

1. *Wing W.* The wing plan-form is untapered, of sweepback $\Lambda = 45$ deg, and of gross aspect ratio 2·4 giving a net aspect ratio $A = 2$, with the chord $c = 0{\cdot}25$; the wing section is biconvex parabolic, of constant thickness/chord ratio $\tau = 0{\cdot}0743$. The complete (gross) wing is located so that its foremost point is a distance 0·35 from the nose of a body; the tip trailing edges are then 0·1 from the base of a body (Fig. 1).

The equation of the complete wing is thus

$$\frac{z}{c} = \tau . 2m(1-m), \quad m = \frac{(x-0{\cdot}35)-y}{c}. \qquad \begin{cases} 0{\cdot}35 \leqslant x \leqslant 0{\cdot}9 \\ 0 \leqslant y \leqslant 0{\cdot}3 \\ 0 \leqslant m \leqslant 1 \end{cases}$$

The area distribution of the exposed wing is

$$S_W(x) = \begin{cases} 0{\cdot}19813(x-0{\cdot}4)^2[1{\cdot}5-4(x-0{\cdot}4)], & 0{\cdot}4 \leqslant x \leqslant 0{\cdot}65 \\ 0{\cdot}19813(0{\cdot}9-x)^2[1{\cdot}5-4(0{\cdot}9-x)], & 0{\cdot}65 \leqslant x \leqslant 0{\cdot}9 \\ 0 \qquad\qquad\qquad\qquad\qquad\qquad , & \text{elsewhere,} \end{cases}$$

and the volume of the exposed wing is

$$V_W = 0{\cdot}0015478.$$

2. *Model* 1. The body of Model 1 has a circular cross-section and has a thickness/length ratio $t = 0{\cdot}1$. It is cylindrical over the rear 0·8 of its length, the nose being the optimum shell shape for given length and base area (Fig. 4a).

The equation of the body B is

$$R_B(x) = \begin{cases} \left[\frac{1}{\pi} S_B(x)\right]^{1/2}, & 0 \leqslant x \leqslant 0{\cdot}2 \\ 0{\cdot}05 \quad , & 0{\cdot}2 \leqslant x \leqslant 1 \end{cases}$$

and its area distribution is

$$S_B(x) = \begin{cases} \frac{1}{200}[\sin^{-1}(5x)^{1/2} + (10x-1)(5x)^{1/2}(1-5x)^{1/2}], & 0 \leqslant x \leqslant 0{\cdot}2 \\ 0{\cdot}0078540 \qquad\qquad\qquad\qquad , & 0{\cdot}2 \leqslant x \leqslant 1 \end{cases}$$

so that its volume is $V_B = 0{\cdot}0070685$

and its base area is $T = 0{\cdot}0078540.$

All other bodies are designed to have the same (unit) length, volume V_B and base area T as this basic body, and to be cylindrical at the base.

---

* A list of symbols is given at the end of Appendix I.

3. *Model* 2. Model 2 consists of the wing W and the body of revolution which is the body of unit length, volume V_B and cylindrical base of area T which has the least sonic wave drag of all such bodies; it is defined by

$$\left.\begin{aligned} R_{B2}(x) &= \left[\frac{1}{\pi}S_{B2}(x)\right]^{1/2} \\ S_{B2}(x) &= \frac{1}{\pi}\left[\frac{64}{3}(2V_B-T)x^{3/2}(1-x)^{3/2}+2Tx^{1/2}(1-x)^{1/2}(2x-1)+T\cos^{-1}(1-2x)\right] \end{aligned}\right\} 0\leqslant x\leqslant 1.$$

4. *Model* 3. The optimum area distribution $S_C(x)$ for a combination of unit length, volume V_C and cylindrical base of area T is given by the expression (Fig. 5a)

$$S_C(x)=\frac{1}{\pi}\left[\frac{64}{3}(2V_C-T)x^{3/2}(1-x)^{3/2}+2Tx^{1/2}(1-x)^{1/2}(2x-1)+T\cos^{-1}(1-2x)\right],$$

$$0\leqslant x\leqslant 1.$$

Since the wing area distribution is $S_W(x)$, the body area distribution for Model 3, $S_{B3}(x)$, is

$$S_{B3}(x)=S_C(x)-S_W(x).$$

The further specification of circular cross-sections defines the body radius

$$R_{B3}(x)=\left[\frac{1}{\pi}S_{B3}(x)\right]^{1/2}.$$

5. *Model* 4. Model 4 is a body of revolution with volume V_C, base area T and optimum area distribution $S_C(x)$ (*cf.* Model 3).

6. *Model* 5*s*. The body of this model is designed to be the body of revolution giving minimum wave drag at $M = 1{\cdot}08$. The method of design is to calculate the mean area distribution of the exposed wing at this Mach number, and subtract it from the optimum area distribution for the entire configuration. However, a minor complication arises in the design of this model, and of Models 6s and 7s in that the end of the mean area distribution of the wing is slightly aft of the base of the body. This difficulty is overcome by stipulating that all the bodies should have the same length and volume and base area, and accordingly the mean area distribution of the wing is delimited at the base of the body thereby reducing slightly the total volume of the configuration and increasing slightly the effective base area of the configuration. The optimum area distribution for the entire configuration is then chosen to be the optimum for the given length and decreased volume and increased base area, and the area distribution of the body is obtained by subtracting from this optimum the delimited mean wing area distribution.

In this case, the modified volumes and base areas are:

$$V_C = 0{\cdot}0086163$$

$$T = 0{\cdot}0078610,$$

so that the optimum area distribution of the entire configuration is given by putting these values in the expression for $S_C(x)$ in Section 4.

7. *Model* 6*s*. The body of this model is designed to be the body of revolution giving minimum wave drag at $M = 1{\cdot}17$. The mean area distribution of the wing at this Mach number gives rise to the modified values of volume and base area

$$V_c = 0{\cdot}0086132$$

$$T = 0{\cdot}0080050,$$

from which the mean area distribution of the whole configuration and the area distribution of the body follow.

8. *Model* 7*s*. The body of this model is designed to be the body of revolution giving minimum wave drag at $M = 1{\cdot}41$. The mean area distribution of the wing at this Mach number gives rise to the modified volume and base area

$$V_c = 0{\cdot}0085722$$

$$T = 0{\cdot}0085560,$$

from which the mean area distribution of the whole configuration and the area distribution of the body follow.

9. *Models* 8 *and* 9. These models were designed by J. A. Bagley in accordance with the general principles outlined by Küchemann and Hartley[2]. The detailed calculations were made using an unpublished method developed by Hartley, which is based on linearised supersonic wing theory and on the theory of quasi-cylindrical bodies. At the time the models were designed, calculations could only be made for axisymmetric bodies, and these solutions were used even though the bodies were not axisymmetric. Subsequently, a calculation method has been developed by Bagley which does not have this restriction. Estimated pressure distributions in the wing–body junctions of Models 8, 9 and 10, calculated by the new method are shown in Fig. 24. They differ somewhat from the distributions originally specified, especially in the case of Model 10.

9.1. *Model* 8. This wing–body combination was designed to have zero C_p in the junction at $M = 1{\cdot}05$, and the body was designed on the assumption that wing influence was negligible at the top of the body. The body junction-line was therefore modified to cancel the wing pressure field there; the top-line of the body was not modified and the fuselage cross-section shape was constructed by drawing half-ellipses between the top-line and the junction shape. The forebody has circular cross-section and is of the so-called Sears-Haack profile, defined by:

$$R_{B\,8}(x) = R(x = 0{\cdot}4)\{1-(1-2{\cdot}5x)^2\}^{3/4} \qquad 0 \leqslant x \leqslant 0{\cdot}4.$$

The after-body is derived from the body of revolution having optimum area distribution and given nose area, length and base area which is modified by indenting the shape in the wing plane to cancel the velocity field due to the wing.

It is now known that, even if $C_p = 0$ in the junction so that there is no drag there, there is usually an even greater drag force outside the junction.

9.2. *Model* 9. This wing–body combination was designed to have a junction pressure distribution at $M = 1{\cdot}05$ similar to that on the infinite sheared wing. In designing this model, an attempt was made to allow for the influence of the wing on the body outside the immediate junction region. Calculations suggested that the wing influence at the top of the body was approximately half the wing influence at the junction, and the top-line of the body was therefore designed to cancel that

field. The body cross-sections were taken as half-ellipses above and below the wing, joining the top-line and junction-line shapes. The forebody and afterbody were similarly defined to those of Model 8, but the afterbody was modified to cancel the field of the wing on the top-line and in the plane of the wing.

10. *Model* 10. This model was designed to combine a full sonic-area-rule application with what was thought to be a poor junction shape which contravened the design principles of Küchemann. The body was therefore straight-sided in the plane of the wing, with the top and bottom lines waisted and elliptic cross-sections. The calculated junction pressure distribution in Fig. 24 shows that even this body shape has a considerable influence on the pressure distribution on the wing, and in fact it does not contravene Küchemann's design principles, although it certainly does not satisfy them fully.

LIST OF SYMBOLS—*Appendix I*

c	Chord of an untapered wing
m	Chordwise parameter used in defining section of a swept-back wing
r	Radial co-ordinate in axisymmetrical flow
t	Thickness/length ratio of a body
x	Rectangular co-ordinate along axis of body
y	Rectangular co-ordinate in plane of wing
z	Rectangular co-ordinate perpendicular to plane of wing
A	(Net) aspect ratio of exposed wing
M	Mach number
$R(x)$	Radius distribution of a body of revolution
$S(x)$	Area distribution
T	Base area common to all bodies
V	Volume
λ	Taper-ratio of a wing
τ	Constant thickness-cord ratio of a wing
Λ	Sweepback of an untapered wing

APPENDIX II

Calculation of the Theoretical Wave Drags

The theoretical wave drags were calculated at Mach numbers of $M = 1{\cdot}00$, $1{\cdot}08$, $1{\cdot}17$ and $1{\cdot}41$ corresponding to values of $(M^2-1)^{1/2} = 0$, $0{\cdot}4$, $0{\cdot}6$ and $1{\cdot}0$. Models 3 and 10 had the same theoretical wave drag.

The wave drags were calculated by linearised theory, using the original version of the supersonic area-rule due to Jones[5] and the numerical method of Eminton[6].

The information concerning the wing used in the estimation of wave drag was the same as that already used for the design of the area-rule models. This information consisted of the elemental area distributions of the wing at angles $\theta = 0$, $\pi/8$, $\pi/4$, $3\pi/8$ and $\pi/2$ for each Mach number $M = 1{\cdot}00$, $1{\cdot}08$, $1{\cdot}17$ and $1{\cdot}41$. The elemental area distributions for $M = 1$, and those for $\theta = \pi/2$, for $M = 1{\cdot}08$, $1{\cdot}17$ and $1{\cdot}41$, were all identical with the cross-sectional area distribution of the wing, of course. The elemental area distribution for $\theta = 0$ and $M = 1{\cdot}41$ was not smooth and strictly this invalidated the calculations for $M = 1{\cdot}41$, but in fact the result was merely to reproduce in part the peaks that full linearised theory would have given. The elemental area distribution of a model at a given θ and M was taken as the sum of the appropriate elemental area distribution of the wing and the cross-sectional area distribution of the body.

The wave drag associated with each elemental area distribution was obtained using the DEUCE programme for the 19-point method[6], and then the wave drag for each model at each Mach number was calculated by applying a four-strip formula of numerical integration.

Acknowledgement is due to Miss D. Larsen and Miss S. Millo who carried through all the stages of the calculations.

APPENDIX III

Base-pressure Measurements

1. *Experimental Technique.* The elements of the base-pressure measuring system utilised for this investigation are illustrated in Fig. 25. The pressure-sensing hole in the base is connected to one side of a differential pressure transducer (range ± 6 p.s.i.). The other side of the transducer is connected to a small reservoir contained within the model which is sealed at ground-level ambient pressure immediately before the test vehicle is launched. Since the pressure in the reservoir is effectively monitored while the vehicle is on its launcher and since the time of flight is about ten seconds there is little chance of a spurious result owing to variations in reservoir pressure, providing the sealing is efficient.

Several improvements were made to this basic system as the trials progressed. Thus, results from the first non-separating models indicated that the pressure transducer was being overloaded during the period of rocket burning and an inertia switch was incorporated which sealed the transducer from the base hole until after the rocket motor had ceased to burn (Fig. 25). On the last non-separating models the number of base holes was increased to two and then to three, each hole having its own transducer connected to a common reservoir (Fig. 26).

For the separating models there was no question of overloading the transducer during boost and these models were not equipped with inertia switches. In an attempt to remove doubts arising from the mode of pressure distribution over the base, the separating models were fitted with a 'pepper-pot' base plate and the base pressure was sensed in a chamber immediately behind the base (Fig. 26). Two independent measurements of this chamber pressure were taken in each model. In order to check that this method of base-pressure measurement was not itself a source of the anomalies noted in the results, the base pressure of one model was measured at a single point on the base as well as in the chamber. Two repeat models (Nos. 5s and 7s) were flown with three direct base-pressure measurements as an additional check.

2. *Discussion of Results.* Before going on to discuss the results in detail a brief comment on experimental uncertainty may be appropriate. The usual 'working' figure for the uncertainty of the measuring equipment used in R.A.E. free-flight trials is ± 3 per cent. The effect of such an uncertainty in terms of C_p is illustrated in Fig. 27. The need to accommodate the C_p range at the highest Mach numbers inevitably results in a large error at subsonic Mach numbers. One point to note, however, is that a large part of this error arises from day-to-day variation in the ground recording equipment; the repeatability in individual test vehicles may be better than ± 3 per cent. Fig. 30 illustrates a typical agreement between three transducers recording base pressure in the same vehicle.

A second preliminary to the main discussion concerns the differences in base pressure to be expected between the various body shapes forming this test series. The primary factors affecting the base pressure are the momentum and direction of the boundary layer leaving the base. Obviously these will be affected by the variations in shape along the whole body length but a reasonable assumption is that the major changes arise from the afterbody shape and most of the experimental evidence available is relevant to various afterbody shapes. The afterbody angles for the circular-cross-section models of the present series (meaned over the last 10 per cent of body length) vary between 0·4 deg and 1·2 deg. Evidence on base pressures at these small afterbody angles is non-existent but one can deduce from the tests on afterbody angles of about 5 deg that the base pressures on these vehicles should not differ appreciably from that of a parallel afterbody. The difference should certainly lie within the error limits quoted in Fig. 27.

For ease of discussion the base pressure results have been divided into three groups. In Fig. 27 results from those models which were tested in both separating and non-separating versions (Models 2 and 3) are compared. There is agreement between the base pressure for the two techniques within the quoted accuracy limits but the base pressures on Models 3 and 3s appear to be lower than those of 2 and 2s. However, if one compares these measurements with base pressures taken from a non-separating model with a parallel afterbody this suggests that the result from Model 3s is high; the others all agree within the experimental error.

Base-pressure results from the supersonic-area-rule models (5s, 6s and 7s) are given in Fig. 28. Two of these (5s and 7s) were repeated specifically to clear up base-pressure anomalies. The one gratifying point about this Figure is the good agreement between the original and repeat versions of model 5s; note that this curve is in general agreement with those of Fig. 27. At supersonic speeds there is fair agreement between Models 5s and 6s though 6s exhibits a low subsonic base drag. This may be a reflection of the increased experimental uncertainty in this region. For Model 7s the results from the original test appear quite spurious and at supersonic speeds the repeat test seems to confirm this contention; as for Model 6s, however, the subsonic base drags are low.

Finally in Fig. 29 the base pressures from the remaining (non-separating) models are given. Here again the discrepancies reflect the increase in experimental uncertainty as the velocity decreases.

At supersonic speeds, if one excludes the spurious results from Model 7s, the base pressure values lie within the ± 3 per cent uncertainty band; at subsonic speeds the scatter appears to be rather greater than ± 3 per cent but for the separating vehicles there is the possibility of greater velocity errors to be taken into account in this region.

Unfortunately, although one can explain most of the observed discrepancies in base pressure on the grounds of experimental inaccuracy, the relatively large ratio of base area/wing area for these models means that if the base drags are applied individually to their respective models, discrepancies much larger than could be explained by uncertainties in the measurement of overall drag arise in the subsonic values of $C_{D\,0}$. The overall subsonic drag coefficients for all models are in good agreement. Therefore if one cannot explain the disagreement introduced by the base drags by experimental uncertainties, one must postulate a subsonic drag other than form, skin friction and base which exactly counterbalances the variations in base drag. This seems unlikely.

On the basis of these considerations, we have argued that the most reasonable solution is to assume a mean base drag curve for all models. This is illustrated in Fig. 18. In deriving it the individual results have been weighted crudely to allow for difference in quality of the raw experimental data.

The obvious danger in this procedure is that one may be obscuring genuine though small differences in base drag between models. This risk we have preferred to the manifestly erroneous solution of accepting each base drag measurement at its face value.

APPENDIX IV

A Comment on Design Application

In a study of the aerodynamics of a transonic aircraft[7] Bagley has made use of the concept that by suitably shaping the tips and body junction of a swept wing the wing flow may be kept sub-critical in character up to a free-stream Mach number corresponding to the critical Mach number of the infinite sheared wing (M_{cs}). This implies that the wing wave drag can be suppressed up to M_{cs}. The results from the present investigation may be viewed in the light of this concept but there are a number of qualifications which obscure the main arguments and for this reason the discussion has been removed from the main text.

The situation is summarised in Fig. 31 which is probably best explained by describing each of the individual curves:

(*a*) The highest-drag curve is taken directly from the measurements on Model 2s, *i.e.*, the test wing in combination with the body having 'minimum' drag in isolation. This represents an 'upper-bound' drag, being composed of body drag + wing drag + positive interference drag.

(*b*) Curve (*b*) is the measured result from the 'sheared-wing' model (9).

(*c*) Curve (*c*) is a composite derived by cross-plotting the results from the sonic and supersonic area-rule models (3s, 5s, 6s, 7s) against design Mach number, and taking the minimum value for a series of free-stream Mach numbers. This curve represents a 'lower bound' of the trends measured in the present tests. To achieve such a lower bound would imply a different body shape for each free-stream Mach number though Fig. 21 suggests that a design for $M = 1{\cdot}28$ would achieve a closely similar drag result, if one ignores sonic speed.

(*d*) Curve (*d*) was obtained by summing the drag of the body of Model 2s ('minimum drag body in isolation') and the measured subsonic drag of the test wing (Fig. 23). The body drag was derived from the measurement made on Model 4 (equivalent body) which differs from 2s in having a volume greater by the amount of the wing volume.

This curve represents the Bagley 'lower bound' up to the critical Mach number of the infinite sheared wing ($M = 1{\cdot}08$). At Mach numbers higher than 1·08 Bagley's arguments would suggest a drag increase up to the level of curve (*a*). We note that this lower bound is below that of the area-rule configurations but it must be recalled that the latter do not necessarily present a genuine physical optimum.

It is clear from Fig. 31 that the 'sheared-wing' design has achieved only about 50 per cent of the drag reduction which Bagley's hypothesis would have suggested. The 'minimal' area-rule curve (*c*) lies above curve (*d*) by an amount corresponding to about 20 per cent of the wing wave drag, a result which, as has been demonstrated (Fig. 21), is in general agreement with area-rule theory.

In the absence of measured pressure distributions one can but speculate on the failure of the sheared-wing design to achieve its aim. The obvious and most plausible reason is that the specified flow and pressure requirements were not achieved either because of additional imperfection in the numerical methods of estimating pressure distribution or because the sheared-wing critical Mach number (1·08) is too near the sonic value for this particular application of linearised theory to be applied with confidence. Another possibility is that the specified wing-root conditions were achieved, and were partially nullified by less favourable pressure distributions elsewhere on the wing.

TABLE 1

Summarised Descriptions of Models Flown

Model number	Brief designation	Description
1	Parallel body	The common wing attached to a body having a low-drag nose for 20 per cent of its length, followed by a parallel afterbody. Body fineness ratio 10/1. Intended to establish a datum drag for a configuration with little or no wing–body interference.
2, 2s	Minimum drag body	The common wing attached to a body having the minimum wave drag for its given volume, length and base area.
3, 3s	Sonic area rule (symmetric)	A wing and body combination with the body shaped to give minimum theoretical wave drag (wing + body) at sonic speed.
4	Equivalent body	A body of revolution having the same length, total volume base area and cross-sectional area distribution as Model 3. Hence it should have the same wave drag at $M = 1$. This is the 'equivalent body' of Model 3.
5s (Two models)	Area rule for $M = 1{\cdot}08$	A wing–body combination designed to have minimum wave drag at $M = 1{\cdot}08$.
6s	Area rule for $M = 1{\cdot}17$	Combination designed to have minimum wave drag at $M = 1{\cdot}17$.
7s (Two models)	Area rule for $M = 1{\cdot}41$	Combination designed to have minimum wave drag at $M = 1{\cdot}41$.
8	Zero C_p	The common wing mounted on a body shaped by the method of Küchemann to give zero pressure in the wing–body junction.
9	Sheared wing	As for 8 but the wing–body junction shaped to give a pressure distribution identical with that on the infinite sheared wing equivalent to the common wing.
10	Sonic area rule (asymmetric)	A wing and body combination with the same area distribution as Model 3, *i.e.*, that to give theoretical minimum sonic wave drag, but with the wing–body junction lines parallel. According to area rule the sonic wave drag should be identical with that of Models 3 and 4.
11	Isolated net wing	The net wing common to all models attached to a body of known drag.

The suffix s signifies a separating model

TABLE 2

Body Ordinates

L = Body length; r = Body radius; h = Height of body perpendicular to wing plane; w = Width of body in wing plane; x = Distance along body axis

	Model number													Body sections		
	1	2 and 2s	3 and 3s	4	5s	6s	7s	8		9		10		Model number		
x/L	r/L	$r\ r/L$	r/L	r/L	r/L	r/L	r/L	h/L	w/L	h/L	w/L	h/L	w/L	1 to 7s	8, 9	10
0·00	0·0	0·0	0·0	0·0	0·0	0·0	0·0	0·0	0·0	0·0	0·0	0·0	0·0	↑	↑	↑
0·02	0·01141	0·00702	0·00822	0·00822	0·00822	0·00818	0·00800	0·0096	0·0096	0·0101	0·0101	—	—			
0·04	0·01887	0·01165	0·01364	0·01364	0·01364	0·01357	0·01328	0·0158	0·0158	0·0166	0·0166	0·0157	0·0119			
0·06	0·02512	0·01559	0·01824	0·01824	0·01824	0·01812	0·01776									
0·08	0·03056	0·01910	0·02233	0·02233	0·02233	0·02221	0·02174	0·0255	0·0255	0·0268	0·0268	0·0254	0·0196			
0·10	0·03536	0·02229	0·02603	0·02603	0·02603	0·02590	0·02536									
0·12	0·03958	0·02522	0·02942	0·02942	0·02942	0·02928	0·02867	0·0331	0·0331	0·0349	0·0349	0·0331	0·0261			
0·14	0·04323	0·02793	0·03255	0·03255	0·03255	0·03240	0·03174									
0·16	0·04630	0·03045	0·03545	0·03545	0·03545	0·03529	0·03458	0·0393	0·0393	0·0413	0·0413	0·0395	0·0318			
0·18	0·04868	0·03281	0·03815	0·03815	0·03815	0·03798	0·03723									
0·20	0·05000	0·03500	0·04066	0·04066	0·04066	0·04048	0·03970	0·0442	0·0442	0·0466	0·0466	0·0450	0·0368			
0·22	↑	0·03706	0·04300	0·04300	0·04300	0·04281	0·04200									
0·24		0·03898	0·04517	0·04517	0·04517	0·04498	0·04415	0·0482	0·0482	0·0507	0·0507	0·0496	0·0412			
0·26		0·04078	0·04719	0·04719	0·04719	0·04699	0·04614									
0·28		0·04246	0·04907	0·04907	0·04907	0·04887	0·04801	0·0511	0·0511	0·0538	0·0538	0·0537	0·0450			
0·30		0·04402	0·05081	0·05081	0·05081	0·05061	0·04974									
0·32		0·04548	0·05241	0·05241	0·05241	0·05221	0·05134	0·0532	0·0532	0·0560	0·0560	0·0570	0·0482			
0·34		0·04683	0·05389	0·05389	0·05389	0·05369	0·05282									
0·36		0·04809	0·05525	0·05525	0·05525	0·05505	0·05396	0·0545	0·0545	0·0573	0·0573	0·0603	0·0506			
0·38		0·04924	0·05648	0·05648	0·05648	0·05625	0·05393									
0·40		0·05031	0·05759	0·05759	0·05744	0·05700	0·05336	0·0549	0·0549	0·0578	0·0578	0·0638	0·0520			
0·42		0·05128	0·05829	0·05860	0·05792	0·05704	0·05264	↑	0·0536	0·0577	0·0576	0·0646	↑			
0·44		0·05216	0·05834	0·05949	0·05781	0·05678	0·05184		0·0519	0·0574	0·0566	0·0641				
0·46		0·05296	0·05785	0·06027	0·05719	0·05589	0·05096		0·0499	0·0566	0·0549	0·0625				
0·48		0·05367	0·05691	0·06095	0·05618	0·05442	0·05016		0·0478	0·0557	0·0528	0·0601				
0·50		0·05429	0·05559	0·06152	0·05473	0·05265	0·04941		0·0459	0·0548	0·0502	0·0570				
0·52		0·05484	0·05399	0·06199	0·05293	0·05078	0·04887		0·0443	0·0538	0·0476	0·0535				
0·54		0·05531	0·05219	0·06235	0·05086	0·04914	0·04867		0·0430	0·0530	0·0449	0·0499				
0·56		0·05569	0·05031	0·06261	0·04865	0·04780	0·04923		0·0422	0·0522	0·0425	0·0463				
0·58		0·05600	0·04845	0·06278	0·04650	0·04675	0·05023		0·0418	0·0517	0·0406	0·0431				
0·60		0·05624	0·04672	0·06285	0·04608	0·04644	0·05123		0·0420	0·0514	0·0394	0·0404				
0·62		0·05640	0·04531	0·06282	0·04597	0·04695	0·05216		0·0427	0·0513	0·0390	0·0384				
0·64		0·05650	0·04437	0·06270	0·04610	0·04817	0·05301	0·0549	0·0441	0·0515	0·0398	0·0375				
0·66		0·05652	0·04408	0·06249	0·04724	0·04960	0·05373	0·0548	0·0448	0·0520	0·0399	0·0374				
0·68		0·05647	0·04444	0·06219	0·04889	0·05088	0·05431	0·0547	0·0454	0·0526	0·0400	0·0380				
0·70		0·05636	0·04532	0·06181	0·05011	0·05187	0·05471	0·0546	0·0459	0·0529	0·0402	0·0395				
0·72		0·05618	0·04656	0·06133	0·05079	0·05255	0·05489	0·0543	0·0464	0·0530	0·0404	0·0417				
0·74		0·05594	0·04802	0·06078	0·05134	0·05296	0·05491	0·0541	0·0470	0·0532	0·0408	0·0443				
0·76		0·05565	0·04955	0·06015	0·05182	0·05312	0·05479	0·0538	0·0475	0·0532	0·0412	0·0472				
0·78		0·05530	0·05106	0·05944	0·05222	0·05309	0·05456	0·0536	0·0480	0·0531	0·0416	0·0501				
0·80		0·05489	0·05241	0·05867	0·05257	0·05293	0·05425	0·0533	0·0484	0·0530	0·0422	0·0528				
0·82		0·05444	0·05355	0·05782	0·05280	0·05268	0·05384	0·0530	0·0489	0·0529	0·0428	0·0552				
0·84		0·05395	0·05435	0·05692	0·05293	0·05236	0·05339	0·0527	0·0493	0·0526	0·0435	0·0568				
0·86		0·05343	0·05476	0·05598	0·05291	0·05204	0·05288	0·0524	0·0496	0·0524	0·0443	0·0577				
0·88		0·05288	0·05467	0·05501	0·05273	0·05171	0·05233	0·0522	0·0500	0·0520	0·0451	0·0575				
0·90		0·05231	0·05401	0·05401	0·05241	0·05140	0·05176	0·0519	0·0502	0·0516	0·0460	0·0561	0·0520			
0·92		0·05175	0·05302	0·05302	0·05198	0·05108	0·05121	0·0516	0·0504	0·0511	0·0470	0·0543	0·0518			
0·94		0·05119	0·05206	0·05206	0·05145	0·05074	0·05070	0·0514	0·0506	0·0506	0·0480	0·0528	0·0513			
0·96		0·05068	0·05118	0·05118	0·05088	0·05038	0·05028	0·0512	0·0508	0·0503	0·0490	0·0517	0·0507			
0·98		0·05025	0·05044	0·05044	0·05034	0·05009	0·05003	0·0510	0·0508	0·0501	0·0497	0·0507	0·0502			
1·00	0·05000	0·05000	0·05000	0·05000	0·05000	0·05000	0·05000	0·0509	0·0509	0·0500	0·0500	0·0500	0·0500	↓	↓	↓

Straight (↑ to ↓) — Straight (↑ to ↓) — Straight (↑ to ↓)

Circular ($0 \leqslant x/L \leqslant 0{\cdot}4$) — Elliptical ($0 \leqslant x/L \leqslant 0{\cdot}4$)

Half-ellipses above and below local wing thickness ($0{\cdot}4 \leqslant x/L \leqslant 0{\cdot}64$)

Elliptical ($0{\cdot}64 \leqslant x/L \leqslant 0{\cdot}98$)

Circular

Circular

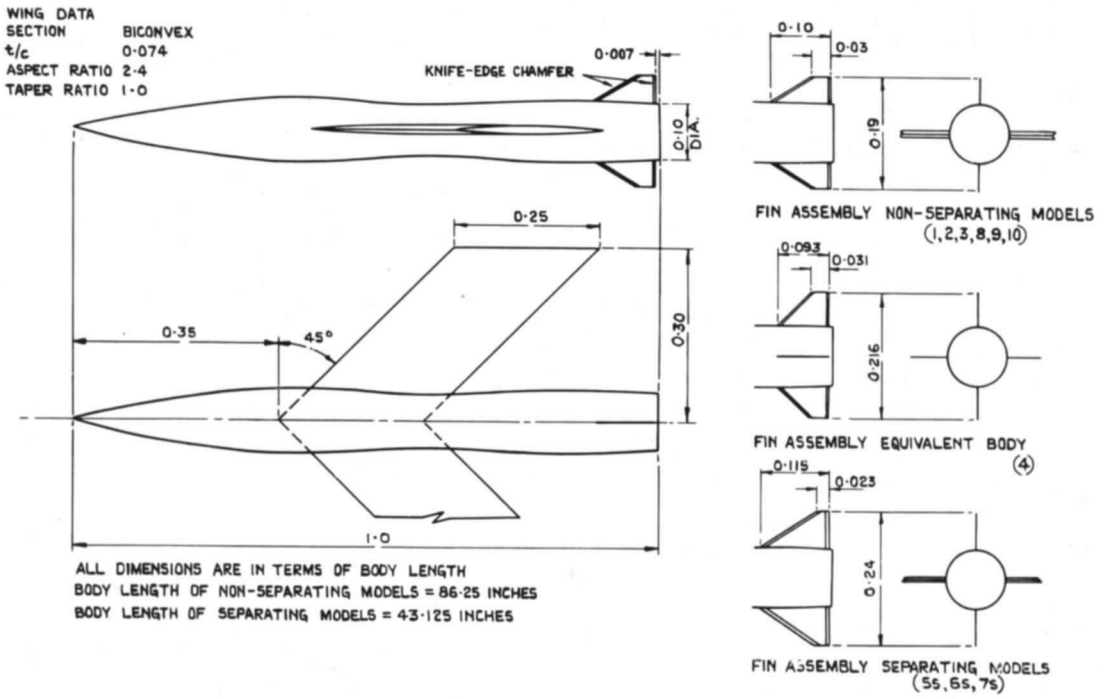

FIG. 1. General arrangement of models.

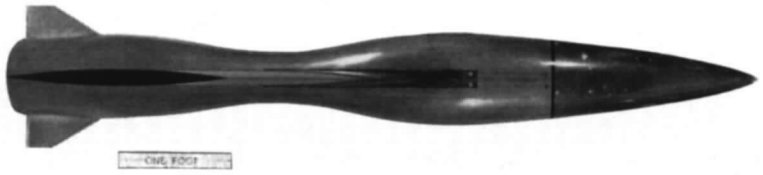

FIG. 2. A typical non-separating model.

FIG. 3. A separating model with boost motor.

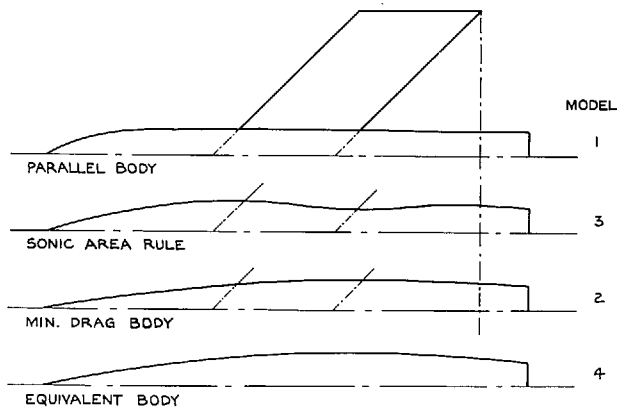

(a) SONIC-AREA-RULE GROUP.

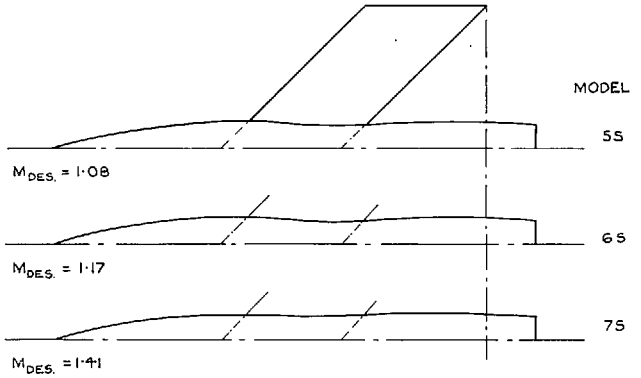

(c) SUPERSONIC-AREA-RULE GROUP.

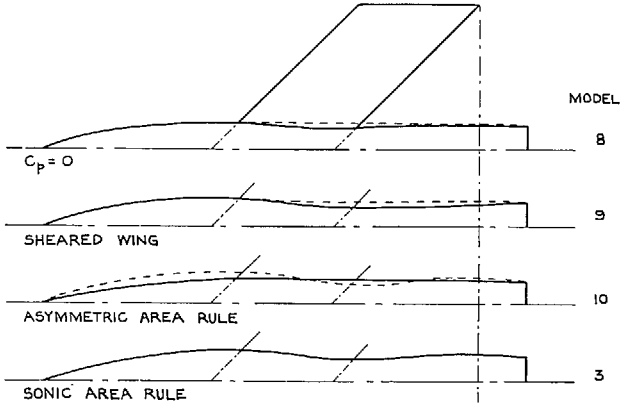

(b) COMPARISON BETWEEN KUCHEMANN AND SONIC-AREA-RULE DESIGNS.

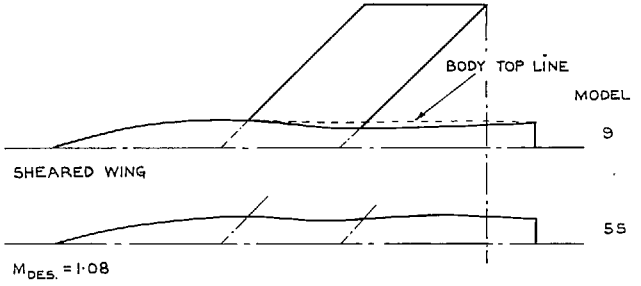

(d) COMPARISON BETWEEN KUCHEMANN AND AREA-RULE. DESIGNS HAVING SIMILAR DRAG CURVES.

FIGS. 4a to 4d. Comparison of body profiles in the wing plane.

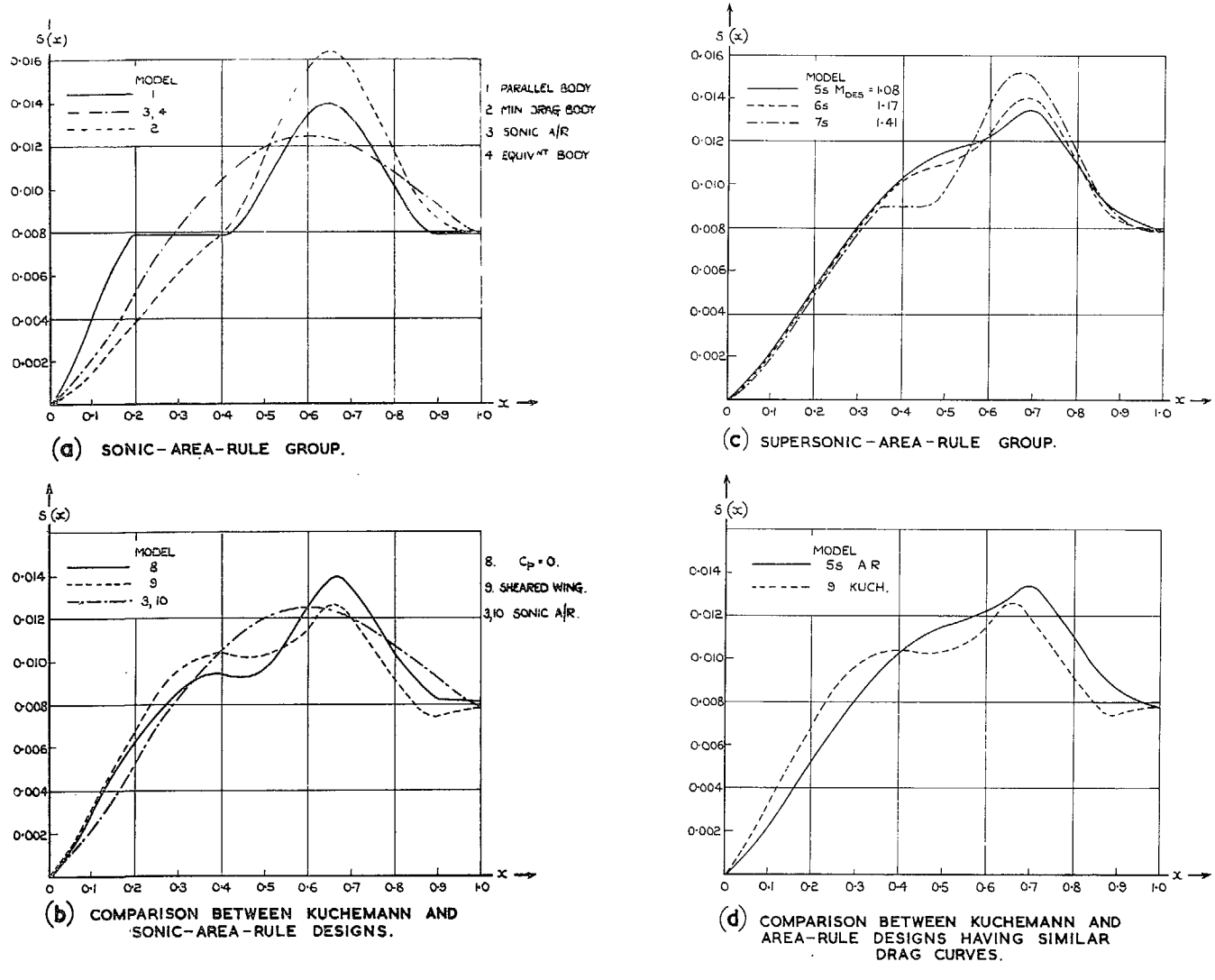

FIGS. 5a to 5d. Cross-sectional area distributions.

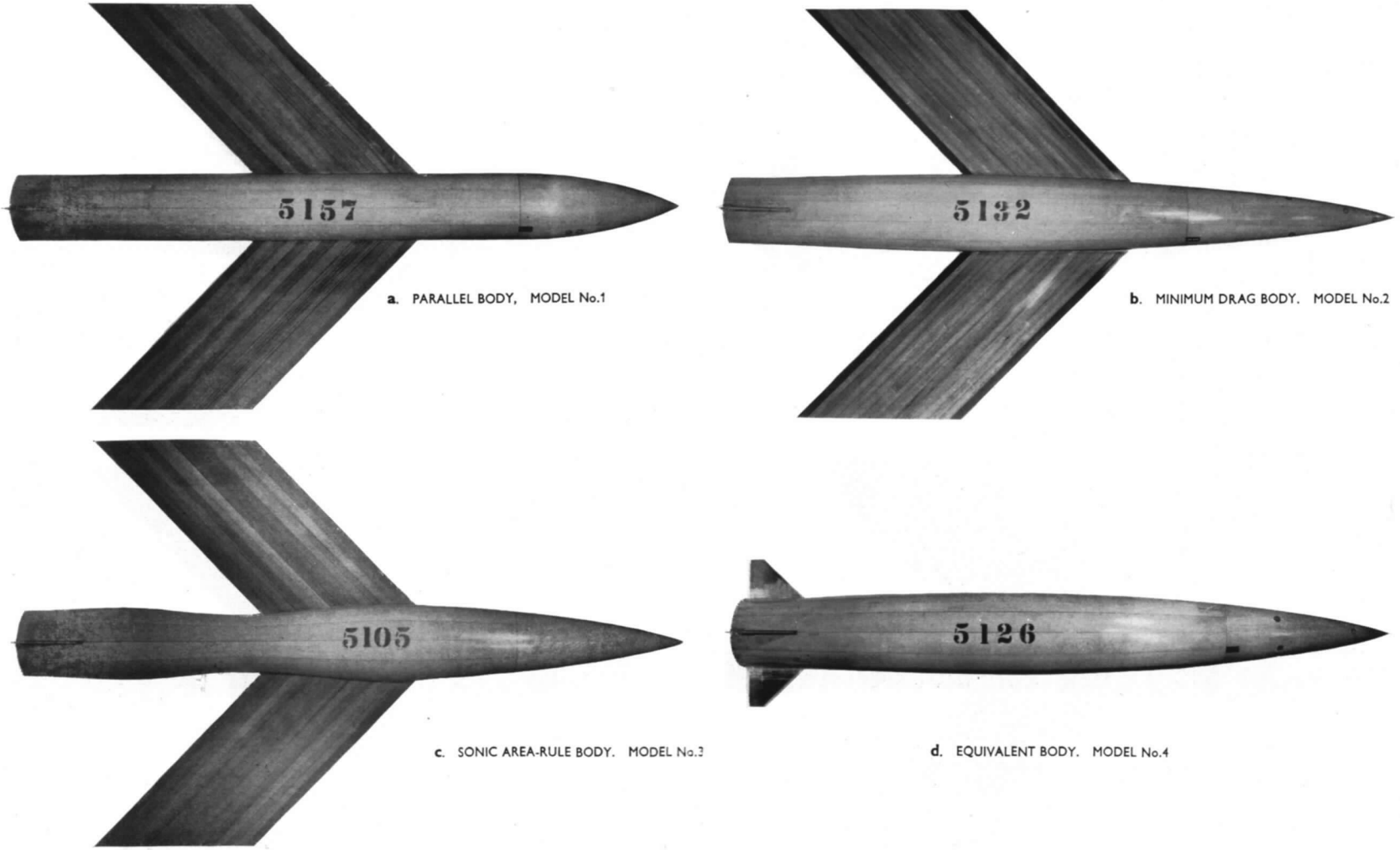

FIG. 6a. Models of the sonic-area-rule group.

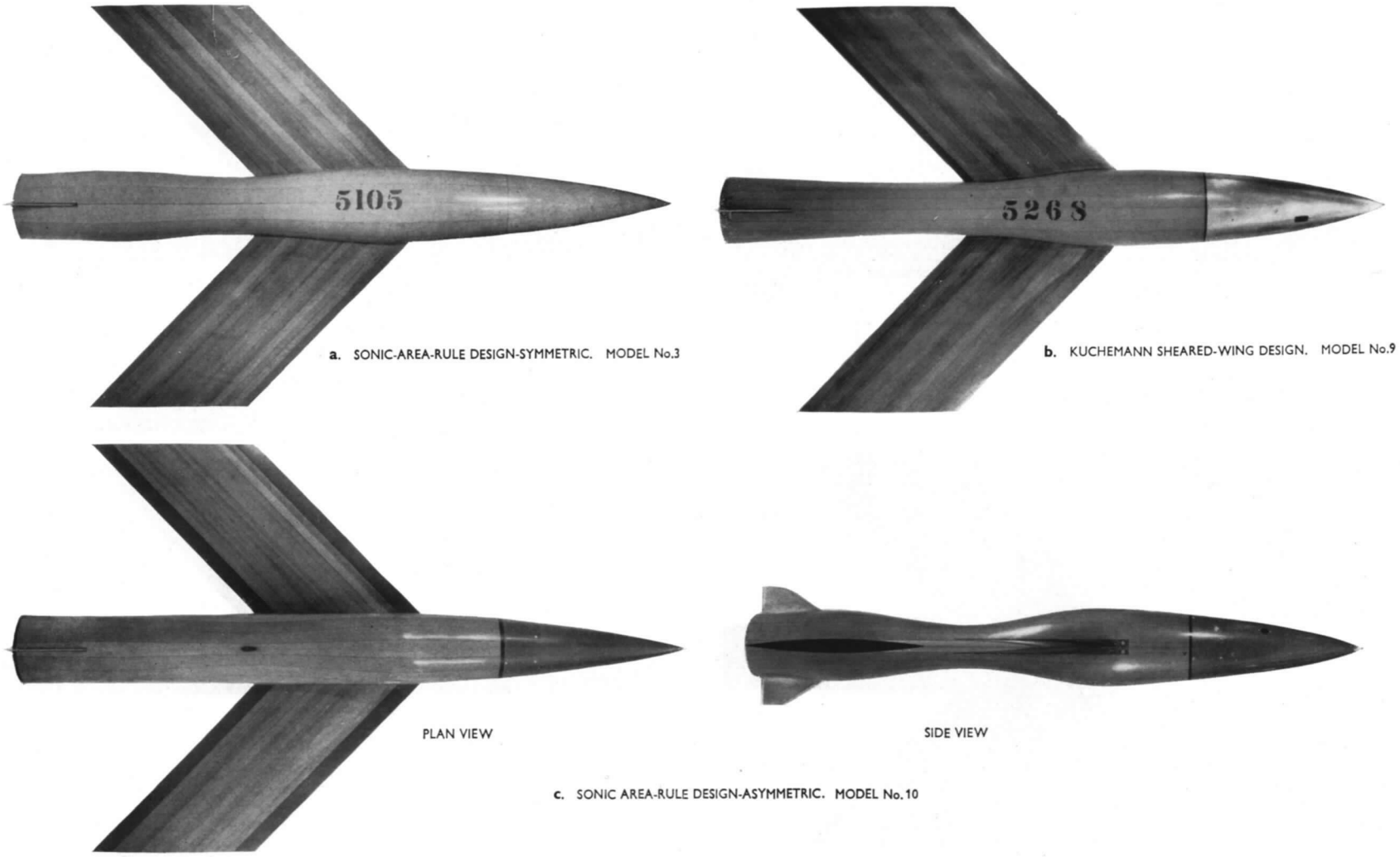

FIG. 6b. Comparison between Küchemann and area-rule models.

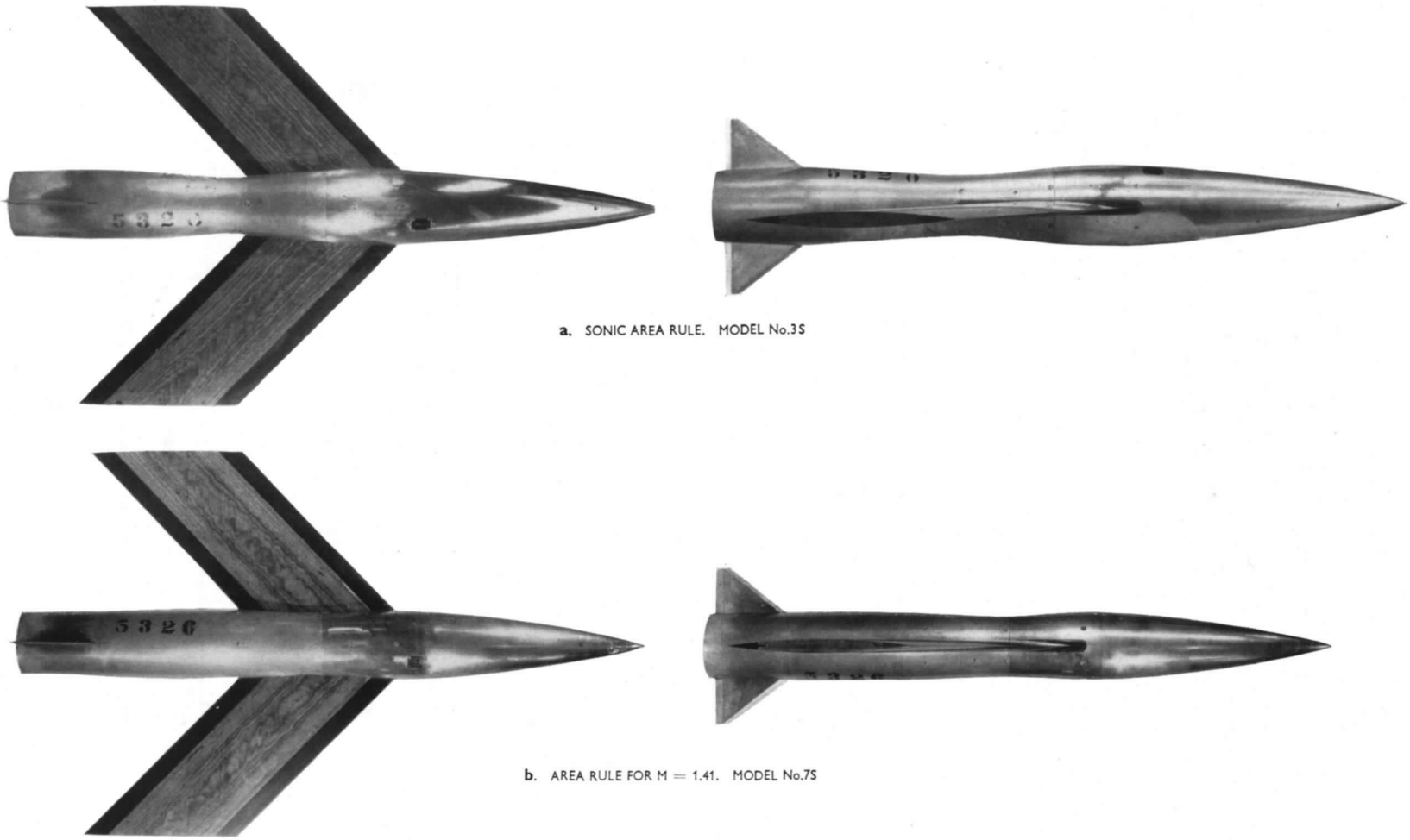

a. SONIC AREA RULE. MODEL No.3S

b. AREA RULE FOR M = 1.41. MODEL No.7S

FIG. 6c. Comparison between sonic and supersonic area-rule models.

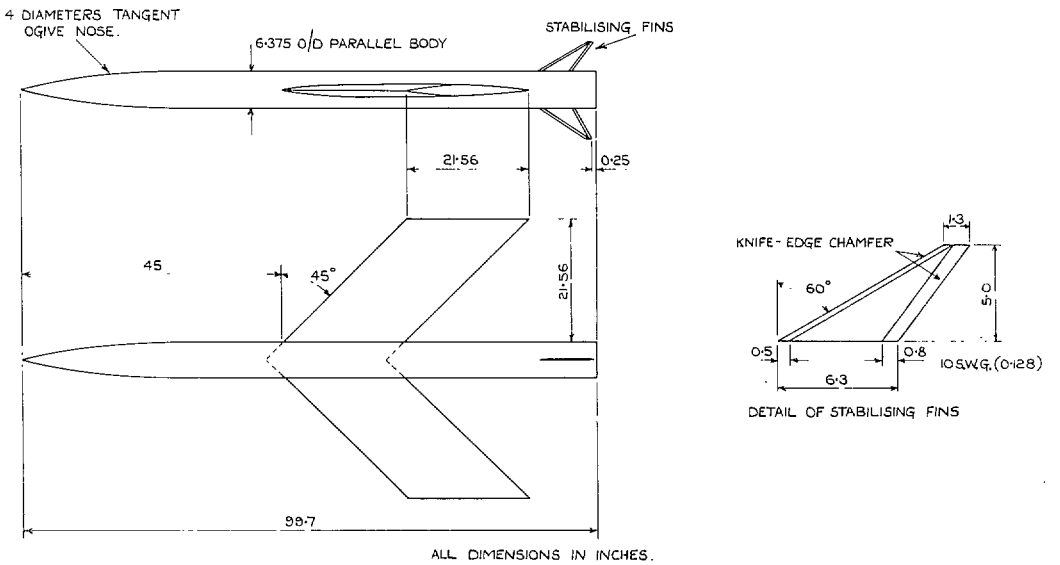

FIG. 7. Test vehicle for measurement of 'isolated net wing' drag (Model 11).

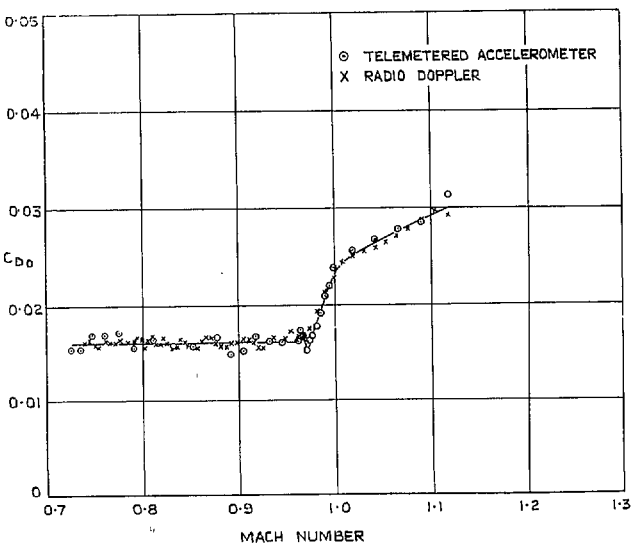

FIG. 8. Comparison between drag measurements derived from accelerometer and radio Doppler.

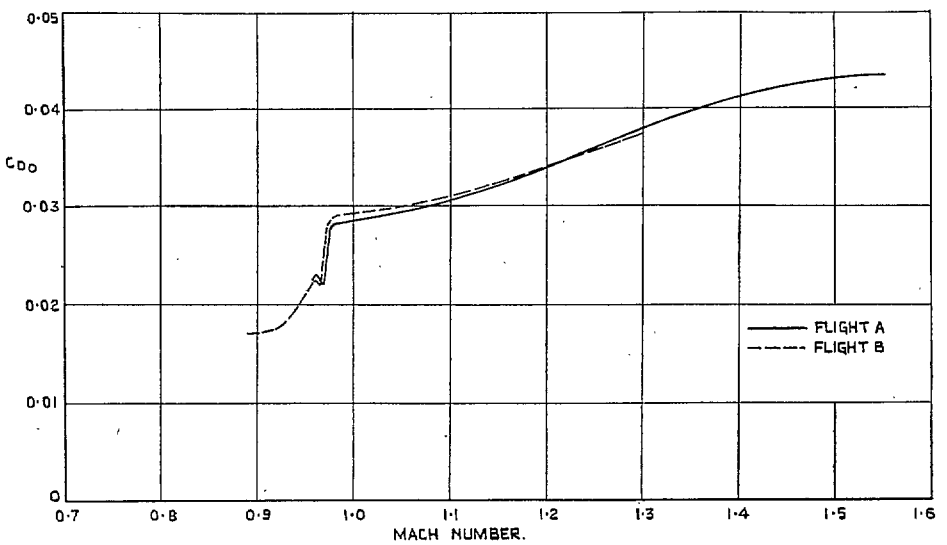

FIG. 9. Comparison between drag results from two tests of Model 5s
(Area-rule design for $M = 1{\cdot}08$.)

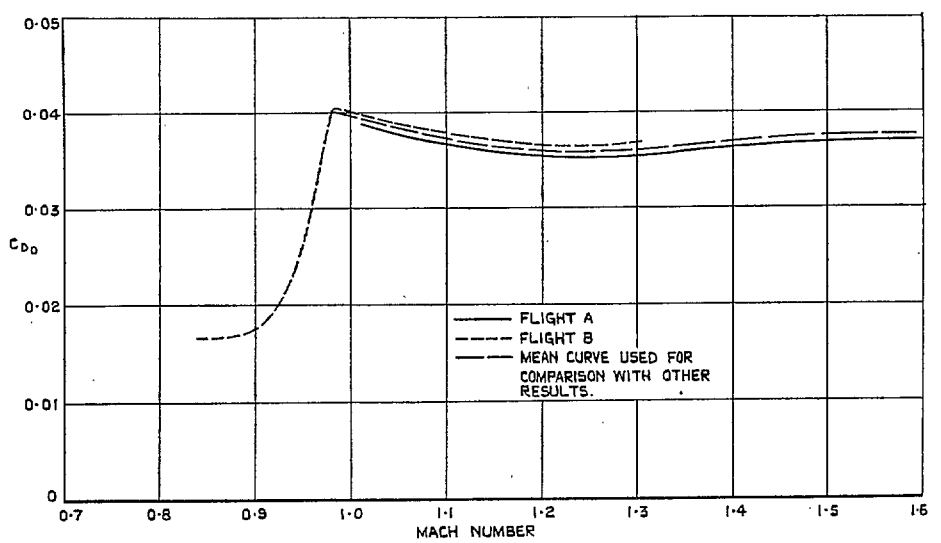

FIG. 10. Comparison between drag results from two tests of Model 7s
(Area-rule design for $M = 1{\cdot}41$.)

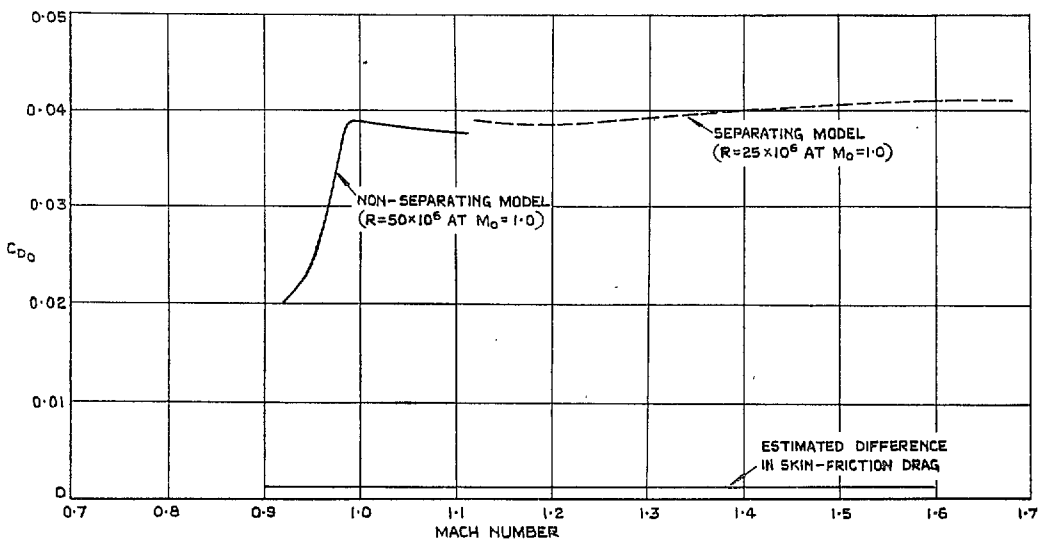

FIG. 11. Comparison between drag results from separating and non-separating versions of Model 2.

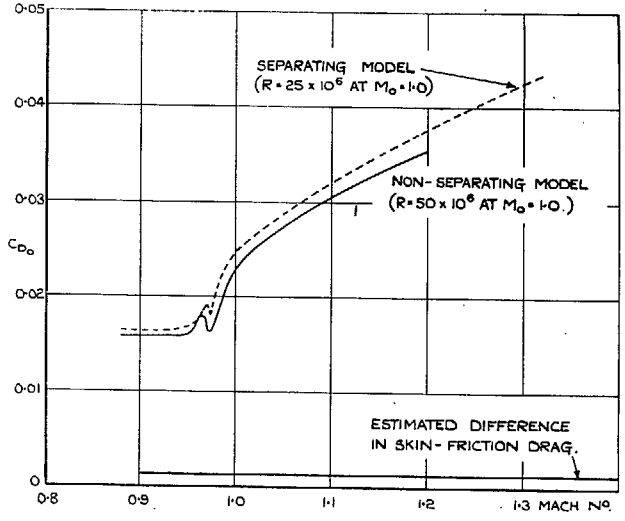

FIG. 12. Comparison between drag results from separating and non-separating versions of Model number 3. (Area-rule design for $M = 1{\cdot}00$.)

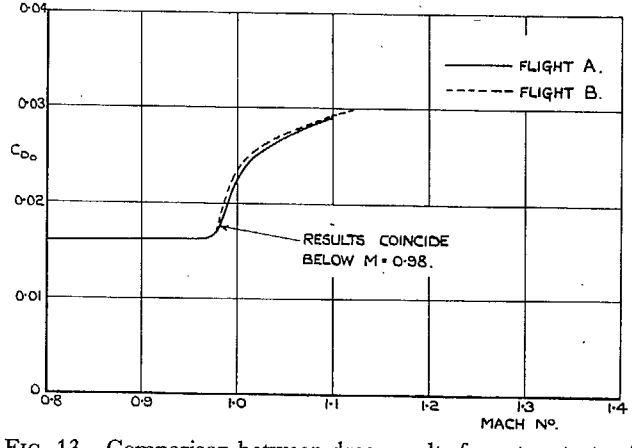

FIG. 13. Comparison between drag results from two tests of Model number 10 (Asymmetric sonic area rule).

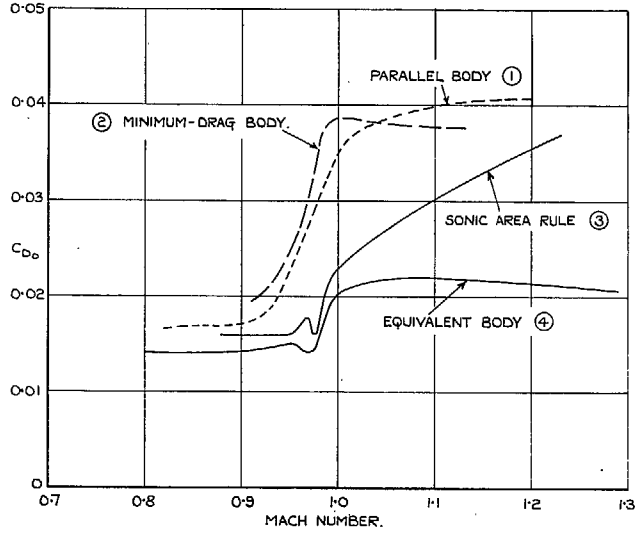

FIG. 14. The effect of sonic area rule on zero-lift drag.

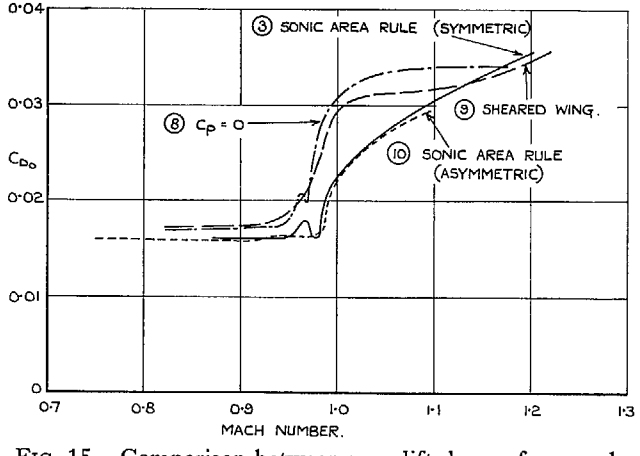

FIG. 15. Comparison between zero-lift drags of area-rule and Küchemann designs.

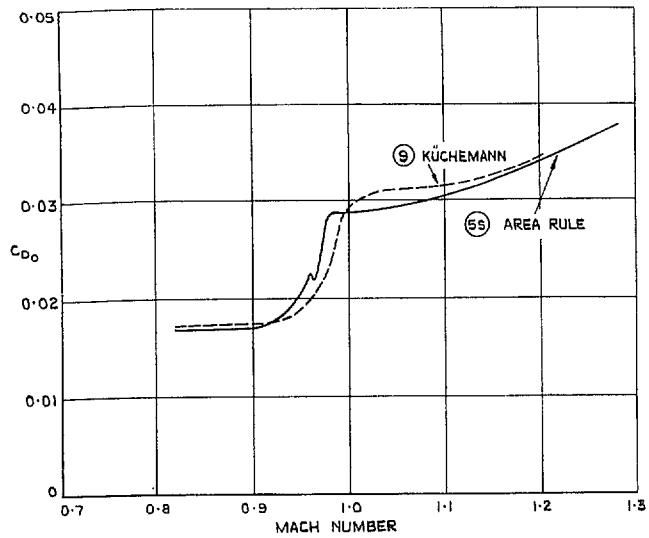

FIG. 16. Drag comparison between a Küchemann design for $M = 1{\cdot}05$ and an area-rule design for $M = 1{\cdot}08$.

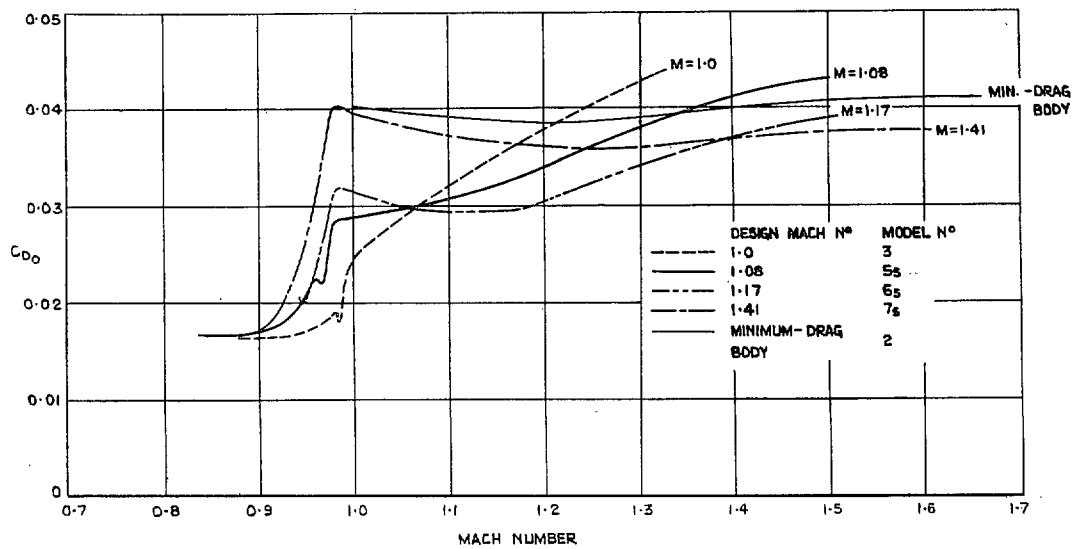

FIG. 17. The effect of area-rule design Mach number on zero-lift drag.

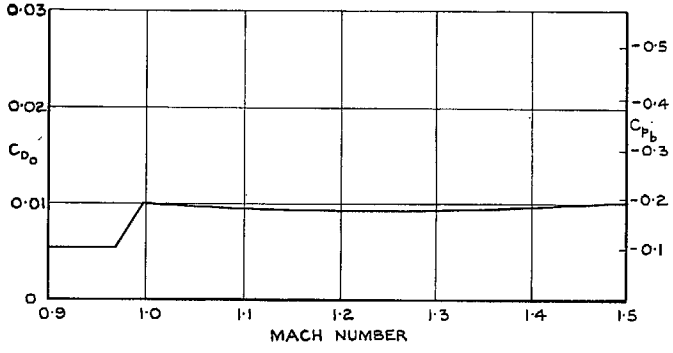

FIG. 18. Variation of base-drag coefficient assumed for theory/experiment comparison (*see* Appendix III).

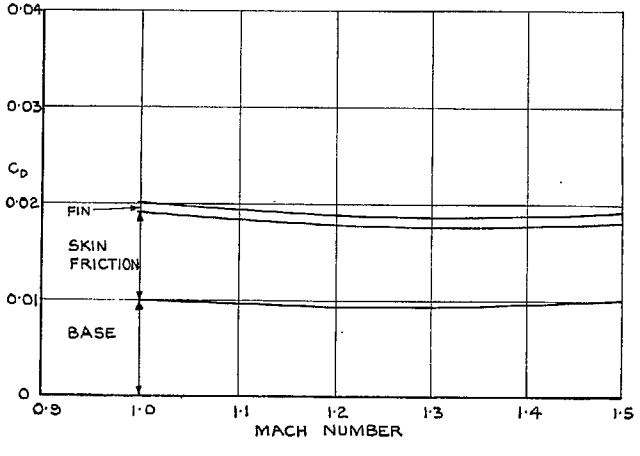

FIG. 19. Extra-to-wave-drag coefficients assumed for theory/experiment comparison.

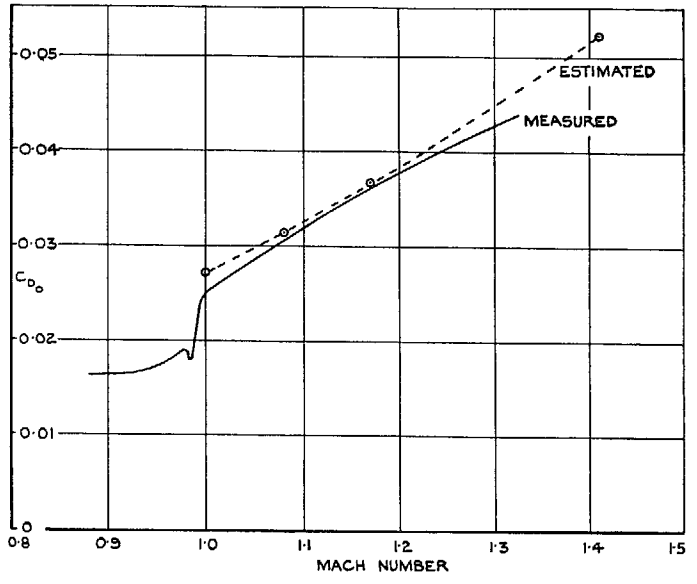

(a) MODEL Nº 3 AREA–RULE DESIGN M = 1·00.

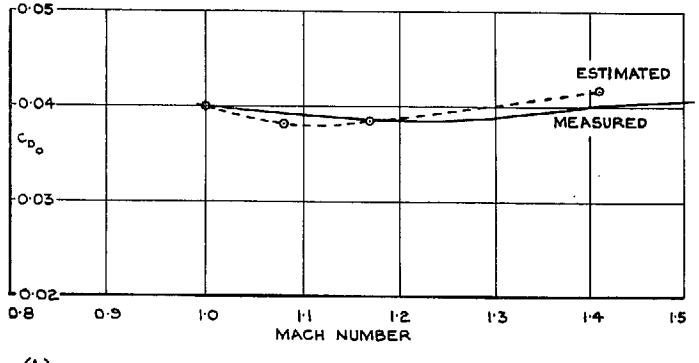

(b) MODEL Nº 2 BASIC WING WITH MINIMUM–DRAG BODY.

FIGS. 20a and 20b. Comparison between measured and estimated values of zero-lift drag.

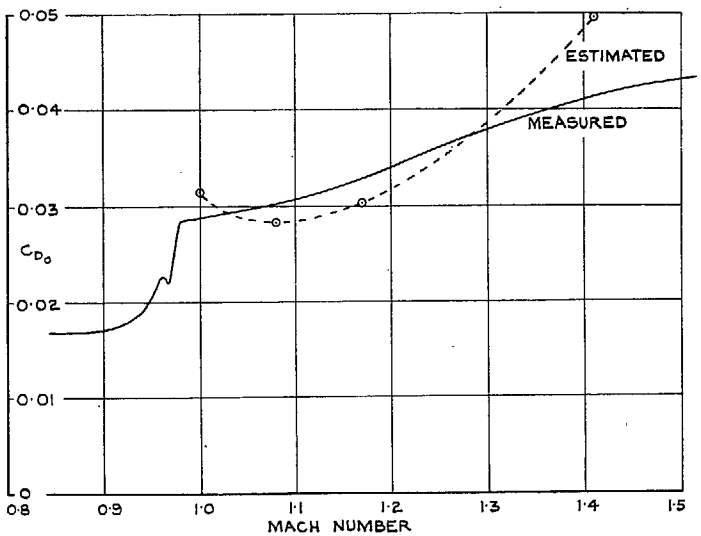

(c) MODEL Nº 5S AREA-RULE DESIGN M = 1·08.

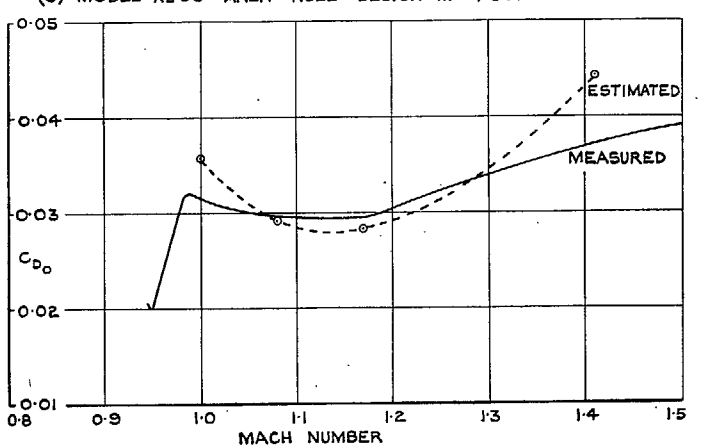

(d) MODEL Nº 6S AREA-RULE DESIGN M = 1·17.

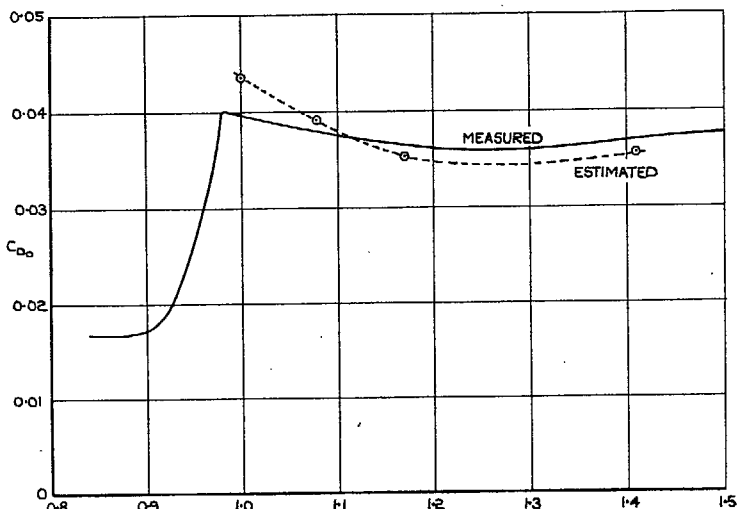

(e) MODEL Nº 7S AREA-RULE DESIGN M=1·41.

FIGS. 20c to 20e. Comparison between measured and estimated values of zero-lift drag.

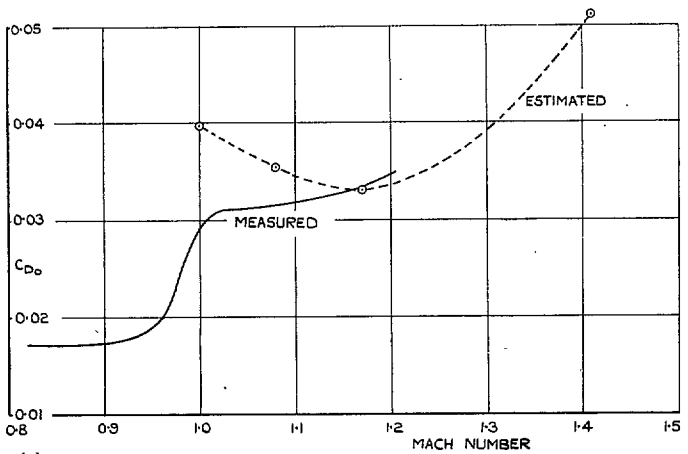

(f) MODEL Nº 9.
KUCHEMANN DESIGN
SHEARED WING.

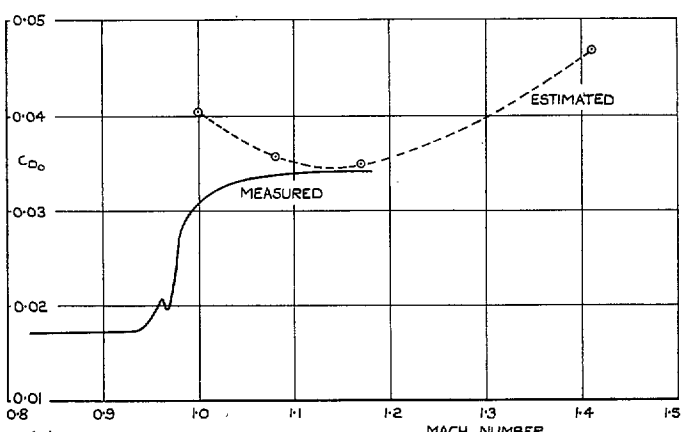

(g) MODEL Nº 8.
KUCHEMANN DESIGN
C_P=O.

FIGS. 20f and 20g. Comparison between measured and estimated values of zero-lift drag.

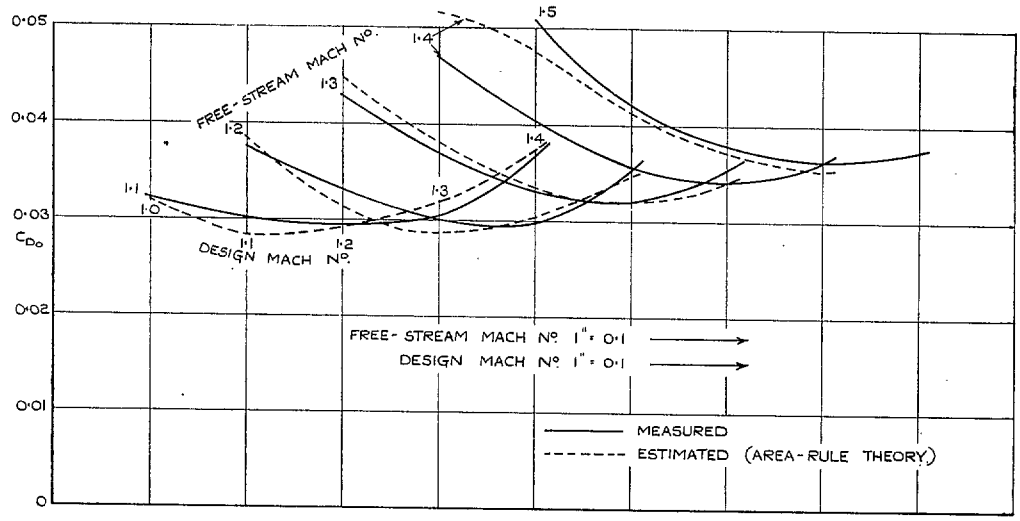

FIG. 21. Carpet of drag variation with area-rule design Mach number and free-stream Mach number.

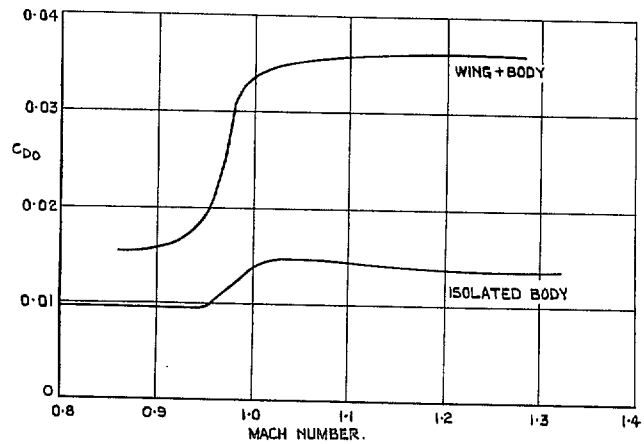

FIG. 22. Drag of Model number 11—Wing + standard drag body.

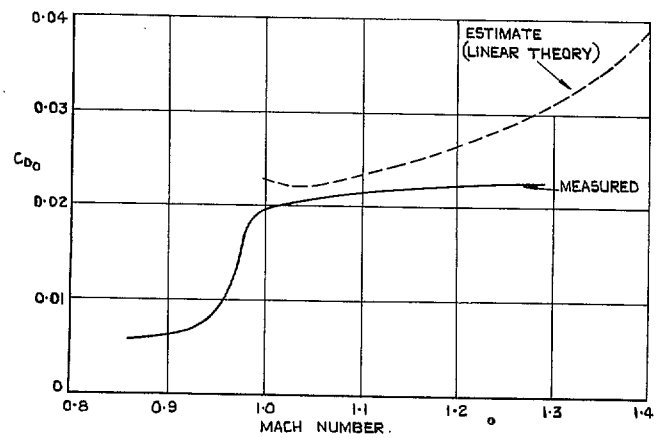

FIG. 23. Drag of the 'isolated net wing' of the present series.
(N.B. $C_{D\,0}$ is based on net wing area in these two Figures.)

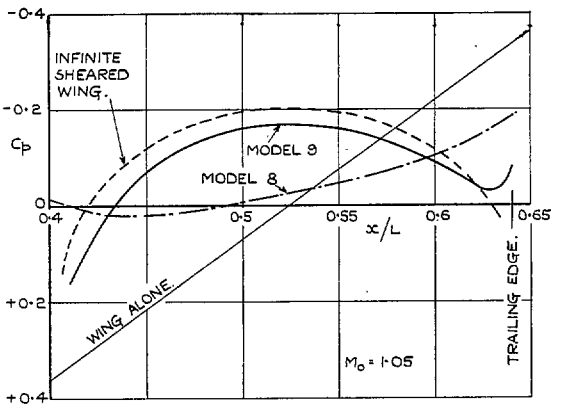

(a) MODELS 8 AND 9.

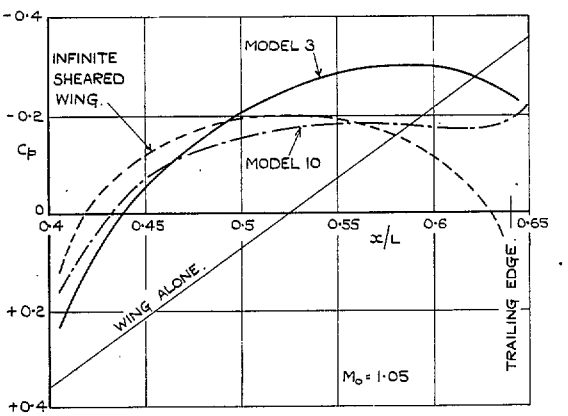

(b) MODELS 3 AND 10 (SONIC AREA RULE DESIGNS.)

FIGS. 24a and 24b. Estimated pressure distributions in junction of various models (Linear theory).

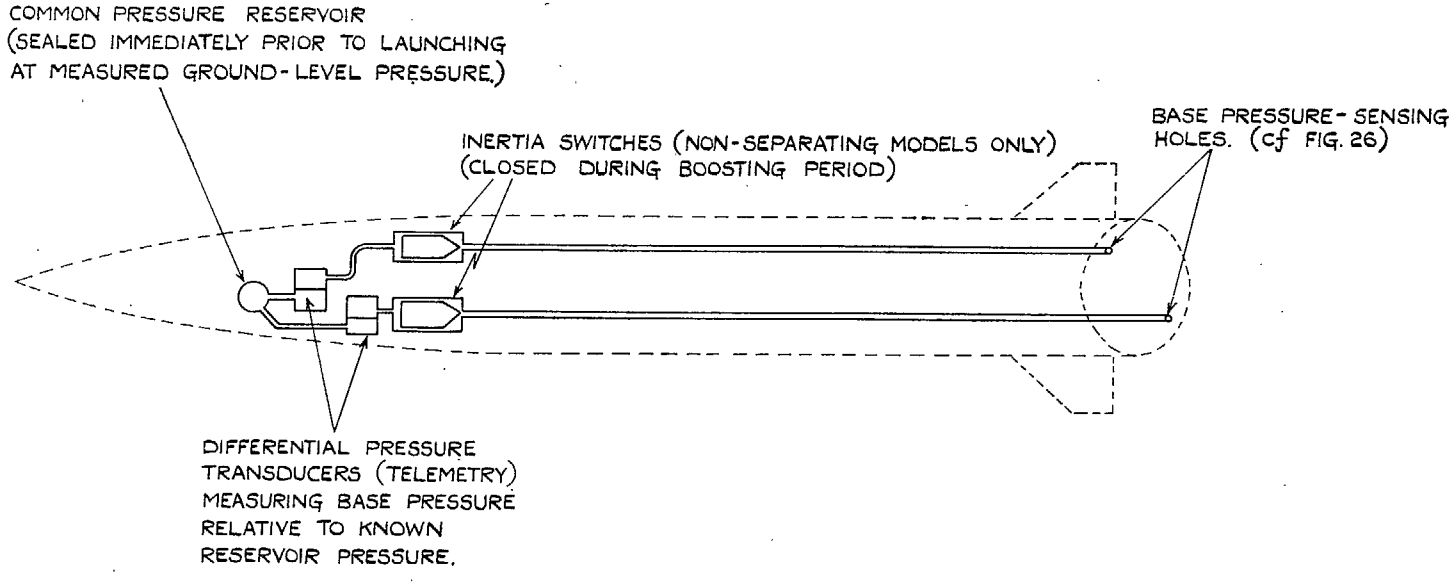

FIG. 25. Base-pressure measuring system (diagrammatic).

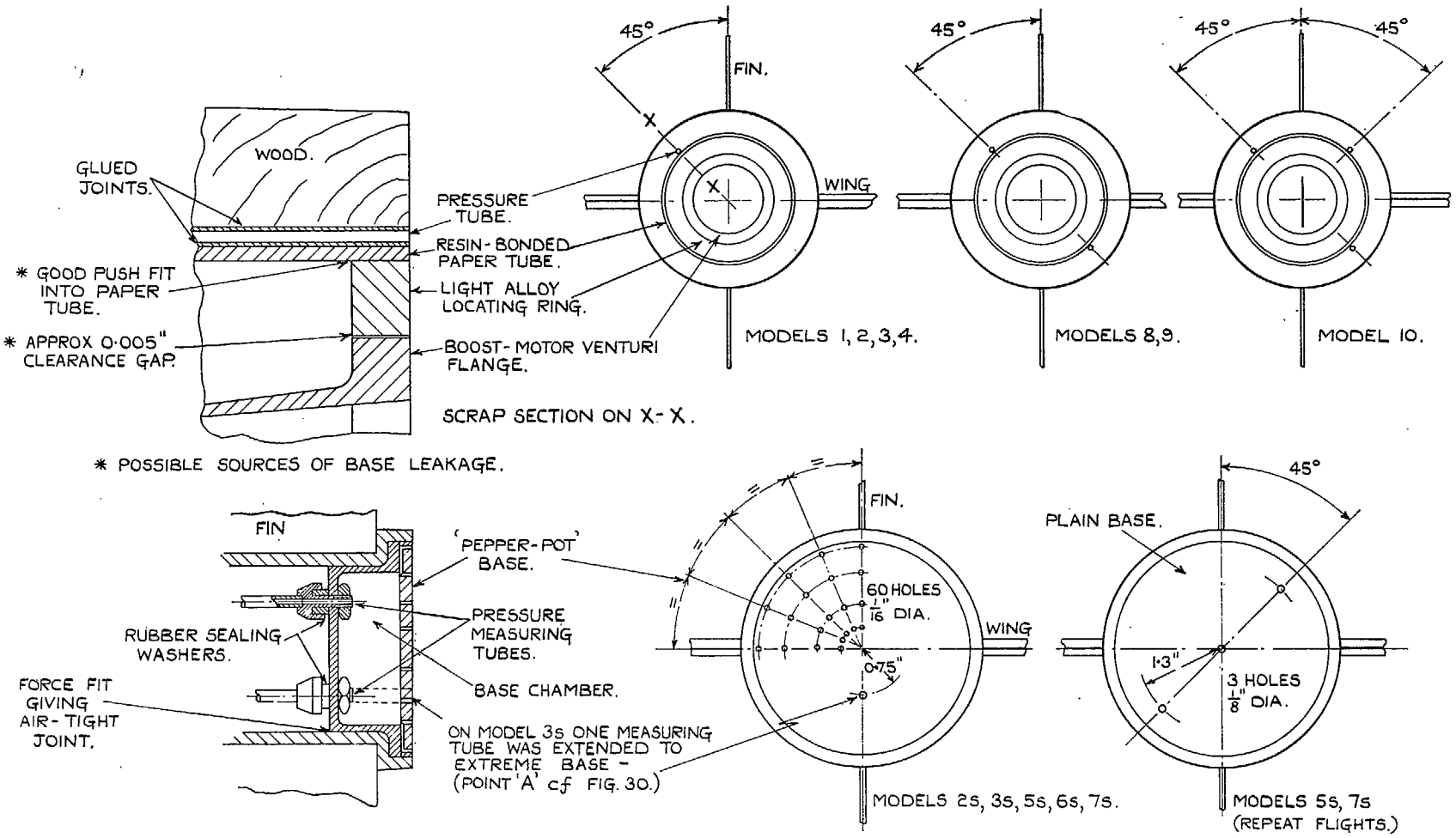

FIG. 26. Methods of measuring base pressure.

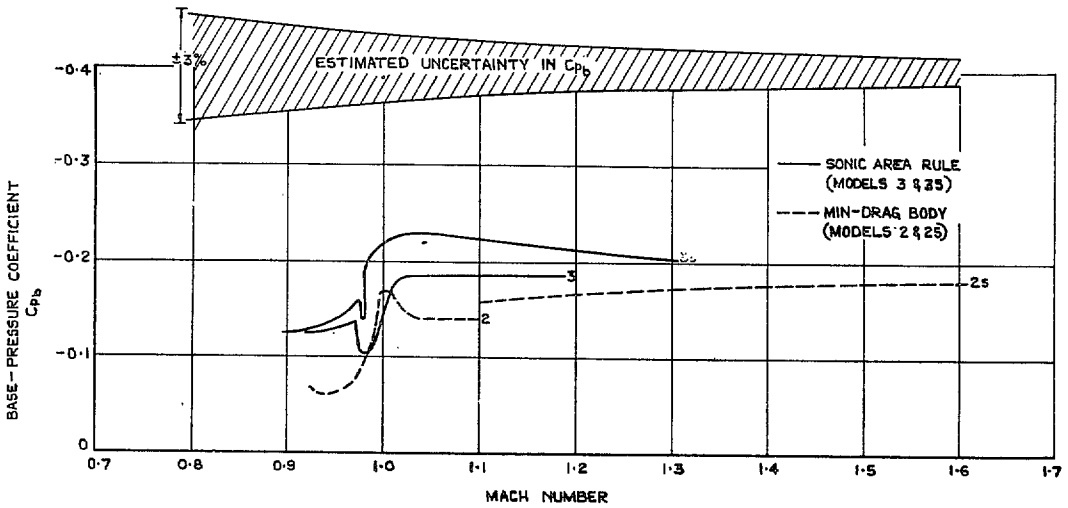

FIG. 27. Comparison between base pressures from separating and non-separating models.

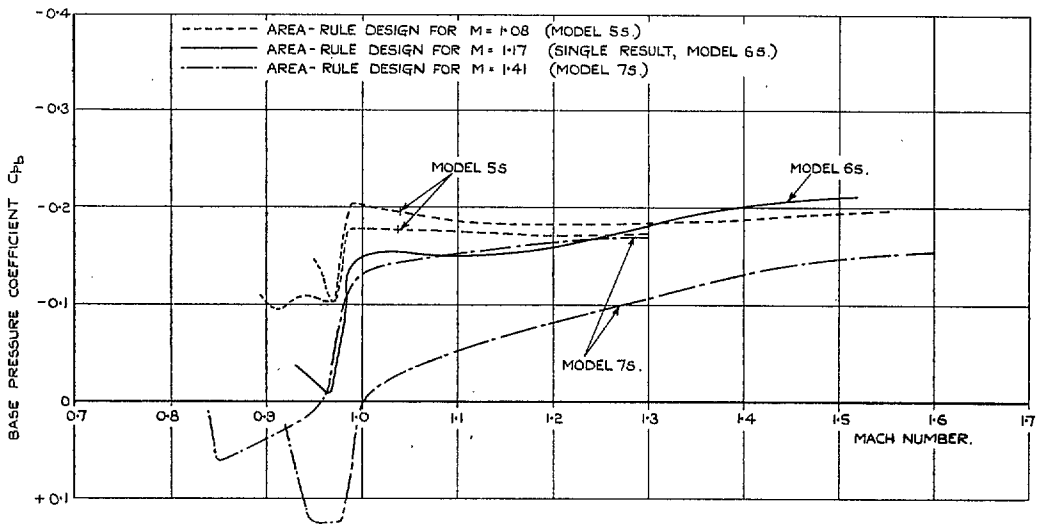

FIG. 28. Comparison between base pressures from repeat tests on identical separating models.

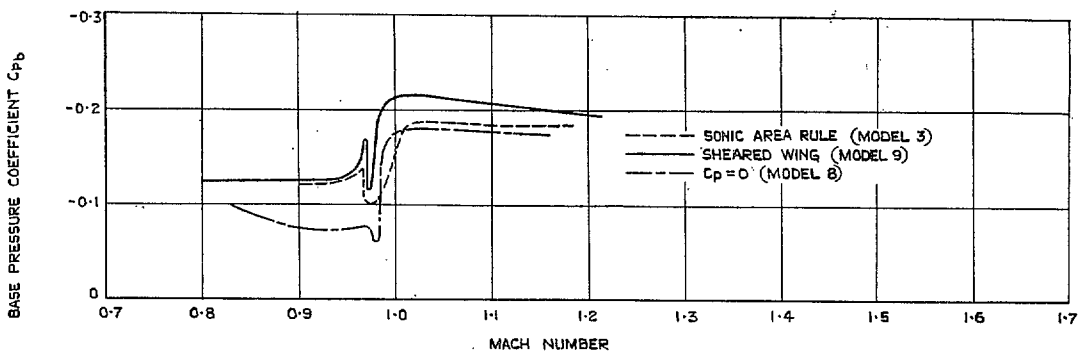

FIG. 29. Comparison between base pressures measured on various non-separating models.

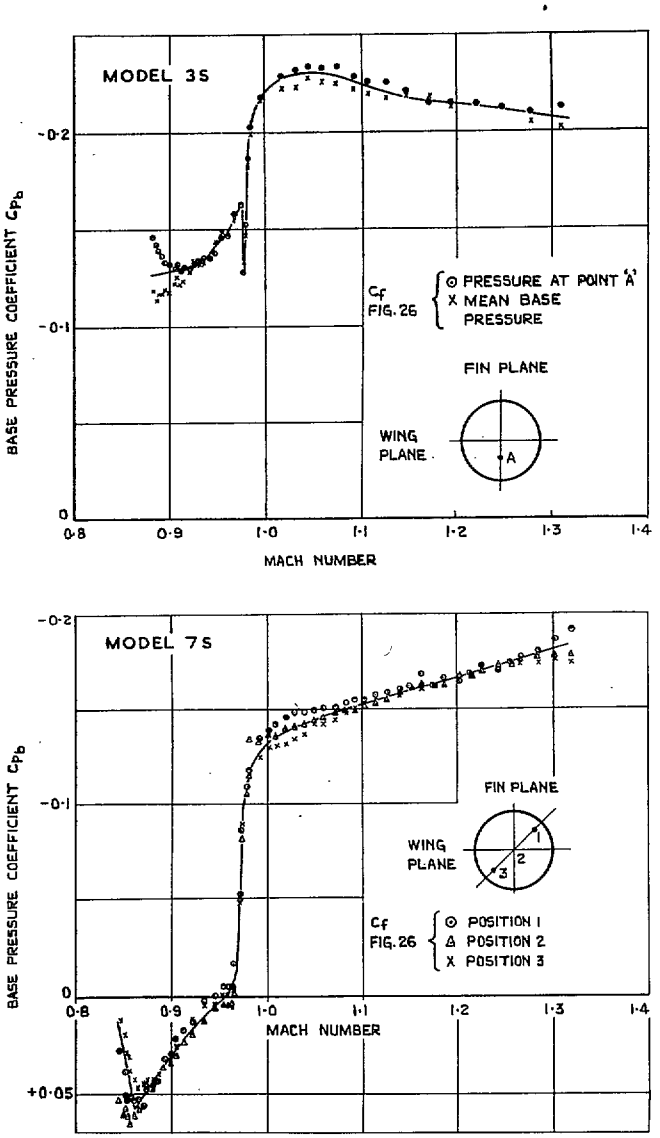

FIG. 30. Typical base-pressure results.

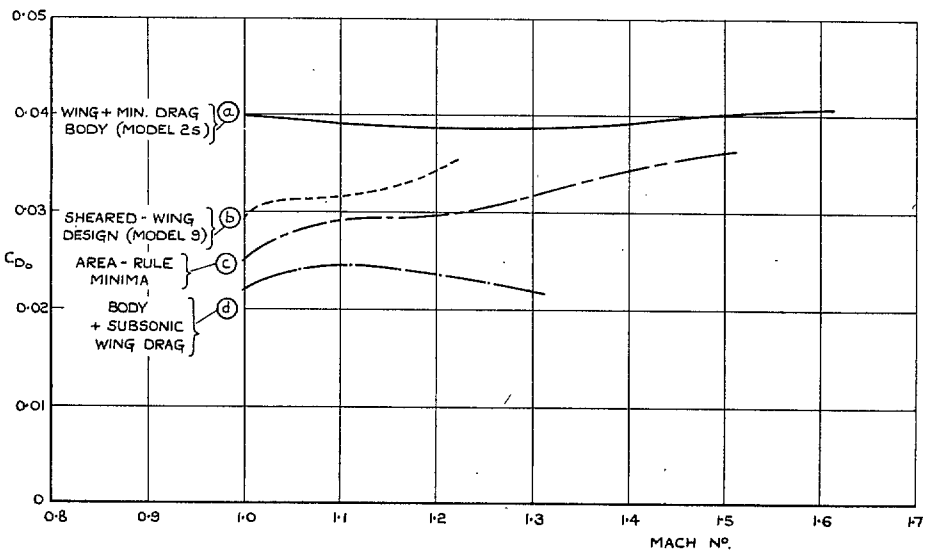

FIG. 31. A comparison between ideal and measured drag.

Wt. 66 K.5.

Printed in England under the authority of Her Majesty's Stationery Office
by John Wright & Sons Ltd. at the Stonebridge Press, Bristol

Publications of the Aeronautical Research Council

ANNUAL TECHNICAL REPORTS OF THE AERONAUTICAL RESEARCH COUNCIL (BOUND VOLUMES)

1941 Aero and Hydrodynamics, Aerofoils, Airscrews, Engines, Flutter, Stability and Control, Structures. 63*s.* (post 2*s.* 3*d.*)

1942 Vol. I. Aero and Hydrodynamics, Aerofoils, Airscrews, Engines. 75*s.* (post 2*s.* 3*d.*)
Vol. II. Noise, Parachutes, Stability and Control, Structures, Vibration, Wind Tunnels. 47*s.* 6*d.* (post 1*s.* 9*d.*)

1943 Vol. I. Aerodynamics, Aerofoils, Airscrews. 80*s.* (post 2*s.*)
Vol. II. Engines, Flutter, Materials, Parachutes, Performance, Stability and Control, Structures. 90*s.* (post 2*s.* 3*d.*)

1944 Vol. I. Aero and Hydrodynamics, Aerofoils, Aircraft, Airscrews, Controls. 84*s.* (post 2*s.* 6*d.*)
Vol. II. Flutter and Vibration, Materials, Miscellaneous, Navigation, Parachutes, Performance, Plates and Panels, Stability, Structures, Test Equipment, Wind Tunnels. 84*s.* (post 2*s.* 6*d.*)

1945 Vol. I. Aero and Hydrodynamics, Aerofoils. 130*s.* (post 3*s.*)
Vol. II. Aircraft, Airscrews, Controls. 130*s.* (post 3*s.*)
Vol. III. Flutter and Vibration, Instruments, Miscellaneous, Parachutes, Plates and Panels, Propulsion. 130*s.* (post 2*s.* 9*d.*)
Vol. IV. Stability, Structures, Wind Tunnels, Wind Tunnel Technique. 130*s.* (post 2*s.* 9*d.*)

1946 Vol. I. Accidents, Aerodynamics, Aerofoils and Hydrofoils. 168*s.* (post 3*s.* 3*d.*)
Vol. II. Airscrews, Cabin Cooling, Chemical Hazards, Controls, Flames, Flutter, Helicopters, Instruments and Instrumentation, Interference, Jets, Miscellaneous, Parachutes. 168*s.* (post 2*s.* 9*d.*)
Vol. III. Performance, Propulsion, Seaplanes, Stability, Structures, Wind Tunnels. 168*s.* (post 3*s.* 6*d.*)

1947 Vol. I. Aerodynamics, Aerofoils, Aircraft. 168*s.* (post 3*s.* 3*d.*)
Vol. II. Airscrews and Rotors, Controls, Flutter, Materials, Miscellaneous, Parachutes, Propulsion, Seaplanes, Stability, Structures, Take-off and Landing. 168*s.* (post 3*s.* 3*d.*)

Special Volumes

Vol. I. Aero and Hydrodynamics, Aerofoils, Controls, Flutter, Kites, Parachutes, Performance, Propulsion, Stability. 126*s.* (post 2*s.* 6*d.*)
Vol. II. Aero and Hydrodynamics, Aerofoils, Airscrews, Controls, Flutter, Materials, Miscellaneous, Parachutes, Propulsion, Stability, Structures. 147*s.* (post 2*s.* 6*d.*)
Vol. III. Aero and Hydrodynamics, Aerofoils, Airscrews, Controls, Flutter, Kites, Miscellaneous, Parachutes, Propulsion, Seaplanes, Stability, Structures, Test Equipment. 189*s.* (post 3*s.* 3*d.*)

Reviews of the Aeronautical Research Council

1939–48 3*s.* (post 5*d.*) 1949–54 5*s.* (post 5*d.*)

Index to all Reports and Memoranda published in the Annual Technical Reports

1909–47 R. & M. 2600 6*s.* (post 2*d.*)

Indexes to the Reports and Memoranda of the Aeronautical Research Council

Between Nos. 2351–2449 R. & M. No. 2450 2*s.* (post 2*d.*)
Between Nos. 2451–2549 R. & M. No. 2550 2*s.* 6*d.* (post 2*d.*)
Between Nos. 2551–2649 R. & M. No. 2650 2*s.* 6*d.* (post 2*d.*)
Between Nos. 2651–2749 R. & M. No. 2750 2*s.* 6*d.* (post 2*d.*)
Between Nos. 2751–2849 R. & M. No. 2850 2*s.* 6*d.* (post 2*d.*)
Between Nos. 2851–2949 R. & M. No. 2950 3*s.* (post 2*d.*)

HER MAJESTY'S STATIONERY OFFICE

from the addresses overleaf

Published by
Her Majesty's Stationery Office

To be purchased from
York House, Kingsway, London w.c.2
423 Oxford Street, London w.1
13A Castle Street, Edinburgh 2
109 St. Mary Street, Cardiff
39 King Street, Manchester 2
50 Fairfax Street, Bristol 1
2 Edmund Street, Birmingham 3
80 Chichester Street, Belfast 1
or through any bookseller

R. & M. No. 3193

S.O. Code No. 23–3193